BOND BEHAVIOR BETWEEN STEEL AND HIGH MODULUS CFRP PLATES AT MODERATLEY ELEVATED TEMPERATURES

A Thesis

Presented to the Faculty of the

Department of Civil and Environmental Engineering

University of Houston

In Partial Fulfillment of the

Requirements for the Degree Master of Science in

Civil Engineering

by

Mehmet Ugur SAHIN

December 2014

BOND BEHAVIOR BETWEEN STEEL AND HIGH MODULUS CFRP PLATES AT MODERATELY ELEVATED TEMPERATURES

Mehmet Ugur SAHIN

Approved:

Chair of the Committee
Mina Dawood, Assistant Professor,
Civil and Environmental Engineering

Committee Members:

Bora Gencturk, Assistant Professor,
Civil and Environmental Engineering

Ken W. White, Professor,
Mechanical Engineering

Suresh K. Khator, Associate Dean,
Cullen College of Engineering

Roberto Ballarini, Professor,
Department Chair

ACKNOWLEDGEMENTS

I would like to express my profound appreciation to my advisor, Dr. Mina Dawood for his tireless guidance and valuable suggestions during this study. It is a great honor to work with such a great academician who wants to share his knowledge and his personal experience with his students. I would not have been able to finish my study without his unflagging patience and favor.

I also would like to thank Dr. Bora Gencturk and Dr. Kenneth W. White for kindly accepting to be a member of my thesis committee.

I would like to acknowledge Mitsubishi Plastic Composites America Inc. for the donation of the carbon fiber materials. The financial support of the Turkish Petroleum Pipeline Corporation is also appreciated.

I wish to express my acknowledgements to Mr. Gerald McTigret and Dr. Bora Acun for the assistance and technical support during my experimental work.

I would also like to thank all of my fellow graduate students at South Park Annex for their help and friendship. A special thank is extended to my dear friend Mossab Wahba El-Than who provided his help and friendship.

I would like to express my gratitude to my parents for their love and supports. Lastly, I would like to thank my girlfriend, Melis Gokus for her unyielding love and support.

BOND BEHAVIOR BETWEEN STEEL AND HIGH MODULUS CFRP PLATES AT MODERATELY ELEVATED TEMPERATURES

An Abstract

of a

Thesis

Presented to

the Faculty of the Department of Civil and Environmental Engineering

University of Houston

In Partial Fulfillment of the

Requirements for the Degree Master of Science in

Civil Engineering

by

Mehmet Ugur SAHIN

December 2014

ABSTRACT

This thesis presents the findings of a research study that was conducted to assess the effect of moderately elevated temperatures, up to 50^{o}C, on the bond behavior of steel beams strengthened with externally bonded carbon fiber reinforced polymer (CFRP) plates. In the first phase of the research, five steel-CFRP bonded double-lap shear coupons were tested at different temperatures to characterize the bond behavior. In the second phase of testing steel beams were strengthened with different configurations of high modulus CFRP plates and subjected to different combinations of applied load and ambient temperature. The temperature ranges considered were selected to represent typical environmental conditions experienced by many steel bridges and structures in different environments. The parameters that are considered in this study include the length of the CFRP plate and the combined effect of mechanical and thermal load.

TABLE OF CONTENTS

LIST OF FIGURES

LIST OF TABLES

CHAPTER 1 INTRODUCTION

The use of fiber reinforced polymer (FRP) composites in civil infrastructure for repair or strengthening applications has become a popular technique in the past 25 years. The use of FRP for rehabilitation of concrete structures specifically has gained research attention and practical application. By comparison, the use of FRP materials for strengthening and repair of steel structures is a relatively new field that has gained comparably little research attention.

The use of FRP as a technique to repair or strengthen steel structures has several benefits when compared to traditional methods such as welding or bolting of steel plates. FRP materials exhibit high stiffness-to-weight-ratios, good corrosion resistance, low thermal conductivity, and provide ease and speed of installation compared to steel. Additionally, bonded FRP joints produce minimal stress concentrations in the substrate structure and bonding FRP to the structure is a reversible process that results in essentially no risk of damage to the underlying structure.

The development of high modulus carbon reinforced polymers (HM CFRP) is a promising approach to repair since HM CFRP materials have elastic moduli that are more than twice that of structural steel. HM CFRP material can be premanufactured as pultruded plates or produced as dry fiber sheets for application by hand lay-up in retrofit application.

1.1 Research Significance

The behavior of steel beams strengthened with externally bonded CFRP plates subjected to mechanical loading has been researched extensively (Deng et al., 2004, Schnerch et al., 2006, Deng and Lee 2007, Dawood et al., 2007, Schnerch et al., 2007, Rizkalla et al., 2008, and Narmashiri et al., 2011, 2012). Research has also been done to characterize the behavior of bonded joints between steel and CFRP at ambient temperatures (Xia and Teng 2005, Fawzia et al., 2006, 2010, Wu et al., 2012, Yu et al., 2012). However, relatively little research was conducted to evaluate bond behavior at moderately elevated temperatures within the range of temperatures for typical outdoor exposure (Stratford and Cadei 2006, Al-Shawaf et al., 2010, Nguyen et al., 2011, 2012, and Stratford and Bisby 2012). Glass transition temperatures of ambient temperature cure epoxy adhesives that are typically used in structural strengthening applications are within the range of 40^{o}C to 60^{o}C. However, the temperatures at which these adhesives start to soften and exhibit a significant reduction of strength and stiffness is often lower than the reported glass transition temperature and can be in the range of 40^{o}C and 50^{o}C. These temperatures are within the range of expected service temperatures for many structural applications with outdoor exposures. Early research suggests that softening of adhesives can lead to excessive bond slip and reduced bond strengths. Further, some research suggests that differences of coefficients of thermal expansion between steel and CFRP can induce large bond stresses which could potentially lead to a premature debonding failure.

The primary objectives of this study are:

- To quantify the bond strength of bonded joints between HM CFRP plate and steel at temperatures up to 50^{o}C which represents the upper bound of service temperatures for steel structures in most outdoor exposures.
- To characterize the response (stiffness, strength, and evolution of strain) of steel beams that are strengthened with externally bonded CFRP plates subjected to combined mechanical and short-term thermal loading.

1.2 Outline of Thesis

The bond behavior between high modulus CFRP plates and steel at temperatures up to 50^{o}C was investigated through an experimental program consisting of two parts. In the first part, double-lap shear coupons were tested in tension at temperatures of 25^{o}C and 50^{o}C to quantify the effect of temperature on bond strength. In the second part, large-scale steel beams were strengthened with different lengths of externally bonded CFRP plates and tested at temperatures of 25^{o}C, 40^{o}C, and 50^{o}C to characterize the bond behavior under flexural loading conditions. The research effort is described in this thesis in five chapters.

Chapter 2 presents a review of the research related to the effect of temperature on bonded joints between steel and FRP. Additionally, a review of research that has been performed related to the flexural behavior of steel beams strengthened with CFRP materials is presented.

Chapter 3 presents the detail of the experimental program that was conducted to evaluate the bond characteristics of CFRP plates under elevated temperatures. The details of the double-lap shear coupon tests and large-scale beam tests, including material properties, test setups, instrumentation layouts, and testing procedures, are presented.

The result of the experimental program and discussion are presented in Chapter 4. The results of the specimens which were tested at different temperature are discussed separately. Additional details of the experimental results are presented in Appendix A.

The conclusions are summarized, and recommendations for future research are presented in Chapter 5.

CHAPTER 2 LITERATURE REVIEW

Several state-of-the-art review papers related to strengthening steel structures with CFRP materials are available in the literature. Hollaway and Cadei (2002) discussed the in service issues related to advanced polymer composite and metallic adherents. They also mentioned the surface preparation for the metallic and composite adherends, durability of FRP composites: thermal effects, ultraviolet effects, fatigue performance, fire performance, and creep and relaxation effects. Additionally, they summarized some field applications which showed the feasibility of the FRP materials using for strengthening metallic structures.

Zhao and Zhang (2007) summarized several topics related to bond behavior between FRP materials and steel such as different bonding test methods, bond strength prediction, bond-slip relationships, and bond failure modes. They summarized developments in strengthening steel hollow compression members with CFRP materials and fatigue crack propagation in FRP-steel structures. A review related to surface preparation, bond, environmental durability, and fatigue was conducted by Harries and Dawood (2012). Zhao et al., (2013) presented a state-of-the-art review about steel structures strengthened with CFRP. This paper added a review of the effect of dynamic loading and environmental conditions on the bond behavior between steel and CFRP. Fatigue, impact, and earthquake loading were discussed. The influence of environmental factors that affect behavior, such as sub-zero temperature effects, elevated temperature effects, ultraviolet light and sea water was also summarized.

The following sections present the previous experimental and analytical research related to bond behavior between steel and carbon reinforced polymer at room temperature and elevated temperature.

2.1 Double-Lap Shear Coupon and Steel Beam Tests at Room Temperature

Fawzia et al., (2006) tested four double lap shear specimen at room temperature. The specimens were prepared by using three layers of normal modulus CFRP sheets on each side of the joint. Four different bond lengths of 40, 50, 70 and 80 mm were considered. Bond failure was observed as a dominant failure mode for normal modulus CFRP. It was found that the effective length of the tested joints was 75 mm. Increasing the bond length beyond this length did not result in any significant increase in bond strength. The study also described a finite element model which accurately predicted the bond strength

Schnerch et al. (2006) tested 44 small-scale CFRP-strengthened steel beams to evaluate the bond performance of high modulus CFRP plates to steel surfaces. Six different types of commercially available epoxy were considered. For each epoxy the bonded length was varied to identify the critical length required to prevent debonding. The flexural bond experimental results showed that SP Spabond 345 and Weld-On SS620 adhesives had the shortest effective bond length.

Deng and Lee (2007) tested a total of ten beams strengthened with different lengths of CFRP plates to investigate the behavior of strengthened steel beams under static loading. They also investigated how the bond strength was affected by using different types of CFRP plates, tapers at the end of the CFRP plate and adhesive spew fillets. The research findings showed that using longer plates increased the strength of the steel beam because increasing the plate length decreased the peak adhesive stress level near the plate ends thereby increasing the debonding strength.

Narmashiri et al., (2011) tested eight steel beams strengthened with different types and thicknesses of CFRP plates, all with constant bond lengths. They used two different CFRP plates including high modulus CFRP plates and high strength CFRP plates. Four different plate thicknesses of 1.2, 1.4, 2, and 4 mm were considered. All the specimens were tested using a four point bending test setup to evaluate the flexural behavior of strengthened steel beams. It was found that changing the thickness and the type of the CFRP plate changed the failure modes. Furthermore, the researchers found that using thicker high strength CFRP plate increased the capacity of the specimen by 38% while 2 mm thick normal modulus CRPP plate increased the capacity by 29%. Furthermore, for specimens having the same plate thickness, using high strength CFRP plate increased the capacity more than using high modulus CFRP plate.

Wu et al., (2012) tested 13 double-lap shear coupons at room temperature. A total of seven double-lap shear coupons were prepared using different lengths of high modulus pultured CFRP plates and Araldite 420 resin. The rest of the double-lap shear coupons were also prepared using same type of CFRP plate and Sikadur 30 resin. The bond lengths considered for the double-lap coupons were in the range of 30 to 260 mm. It was observed that all of the specimens that were bonded using the Sikadur 30 adhesive exhibited cohesive failure modes while the failure mode of the Araldite specimens shifted from CFRP delamination to CFRP rupture with increasing bond length. It was believed that the change of the observed failure mode depended on the differences of the adhesive stiffness and toughness.

2.2 Double Lap Shear and Steel Beam Tests at Elevated Temperature

Al-Shawaf et al., (2010) conducted experimental research to study the bond behavior between CFRP and steel plates at temperature ranging from 20 to 60^{o}C. A total of 20 double-lap coupons were prepared using a wet layup method using a unidirectional high modulus carbon fiber fabric sheet. Three different types of resin were considered. The total specimen length and total bond length were 302 and 202 mm respectively. It was found that the joint capacity depended on the adhesive type. Changing the adhesive increased the bond strength by between 17 and 30% for the adhesives considered in this study. The results also indicated that the joint capacities decreased by between 35 and 68% when the testing temperature was increased to 60^{o}C. The decrease in bond strength was attributed to the decrease of the adhesive strength at elevated temperatures.

Similarly, Nguyen et al., (2011) tested 63 CFRP and steel double-lap joints at temperatures of 20, 40, and 50^{o}C. The primary testing variables were the bonded length and the number of layers of wet lay-up CFRP sheets. The bonded joints were tested in two groups. In the first group, a total of 39 specimens were tested including 17 coupons with a single layer of CFRP on each side of the double-lap joint and 22 coupons with three layers of CFRP on each side of the double lap joint. The coupons were tested monotonically in tension after reaching the target temperature. The test temperatures of 40 and 50^{o}C were selected to be on either side of the glass transition temperature of the adhesive, which was reported to be 42^{o}C. In the second group, 24 specimens were tested, 12 with one layer of CFRP and 12 with three layers of CFRP specimens. Five different ambient temperatures ranging from 20 to 60^{o}C and two different bond lengths of 60 and 100 mm were considered. Research findings showed that increasing the temperature caused a decrease in the ultimate capacity of the specimens by 15, 50, and 80% compared to the room temperature strength for specimens tested at 40, 50, and 60^{o}C respectively. This was attributed to the deterioration of the shear strength of the adhesive at higher temperatures.

Stratford and Bisby (2012) studied the effect of high temperatures on the behavior of steel beams strengthened with CFRP. A total of six steel beam strengthened with same length of CFRP plate were tested. A sustained load which was greater than the capacity of the unstrengthened beams was applied and the temperature of the beams was increased until failure occurred. The specimens were heated using an electrical heating pad located at one end of the bonded region. All of the tested specimens failed by plate debonding. The results suggested that elevated temperatures can cause premature debonding of FRP plates under the right conditions.

2.3 Analytical Bond Studies

Several analytical studies were conducted to investigate the stress distribution in the adhesive layer of in steel beams strengthened with FRP plates. Deng et al., (2004) presented numerical solution to calculate shear stresses and normal stresses in strengthened beams with tapered and non-tapered CFRP plates subjected to different loading conditions. The approach adopted a finite difference method to predict in the adhesive layer. The model assumed linear elastic material properties for the steel, FRP, and adhesive, and that the stress was constant through the adhesive thickness. It also assumed that debonding failure occurred when the principal stress at the end of the plate reached the ultimate strength of the adhesive. The results showed that using tapered CFRP plates could reduce the normal and shear stresses significantly at the end regions.

A similar analytical approach was proposed by Stratford and Cadei (2006), although this model was limited to plates with square ends. This model provided a solution to calculate the distribution of elastic shear and normal stresses that are induced by static loading, change of temperature and release of plate prestressing. The study suggested that the adhesive stresses induced by temperature changes can be three times higher than the adhesive stresses induced by mechanical loading. However, this study did not consider the change of the adhesive properties due to increasing temperatures. That is, the strength and stiffness of the adhesive at elevated temperatures were assumed to be equal to their room temperature values which could have a significant effect on the predicted stress distributions.

CHAPTER 3 EXPERIMENTAL PROGRAM

This chapter describes the experimental program that was conducted to examine the bond and flexural behavior of the steel beams strengthened with high modulus CFRP plates at test temperatures up to 50^{o}C. The experimental program consisted of two stages. In the first stage, five double-lap shear coupons were tested at different temperatures to evaluate the bond behavior at moderately elevated temperatures. In the second stage, eight large-scale steel beams were strengthened with different lengths of HM CFRP plates and tested at different temperatures to study the behavior of the strengthening system under flexural loading conditions at different temperatures. This chapter presents the details of the double-lap shear coupon tests and the large-scale tests, including the materials, instrumentation layouts, test setups and loading protocols.

3.1 Double-Lap Shear Coupon Tests

In the first stage of the experimental program, five double-lap shear coupons were tested. The aim of these tests was to evaluate the effects of the bond behavior of the HM CFRP strips to steel surfaces at temperatures up to 50^{o}C. Details of the specimen configuration, materials, test set up and instrumentation are described in the following sections.

3.1.1 Test Specimens

The tested double-lap shear coupons, shown Figure in 3.1, consisted of two 19 mm thick x 38 mm wide steel plates which were bonded to together using two 2 mm thick x 38 mm wide CFRP plates. The width of the plates in the 128 mm long grip region was 50 mm. The rest of the plate was machined to a width of 38 mm to prevent premature failure in the grip region.

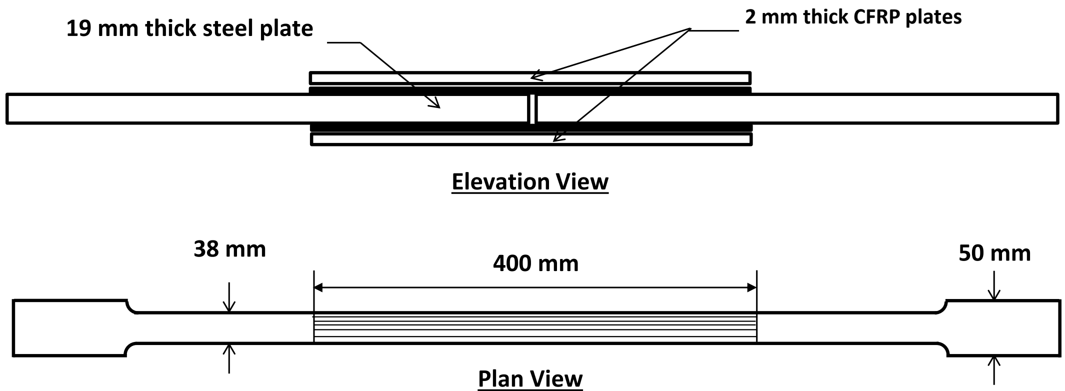

Figure 3.1 Schematic view of double lap shear specimen

The test matrix for the double-lap shear coupon tests is given on Table 3.1. Two different test temperatures, 25 and 50^{o}C, were considered. The repeatability of the test results was evaluated by testing two or three repetitions of each test configuration. Each coupon was assigned a unique two-part identifier. The first part indicates the target test temperature and the second part is a serial number indicating repetition number of the test coupon.

Table 3.1 Test Matrix of Double Lap Shear Tests

Specimen ID	CFRP Length (mm)	Plate End Angle (°)	Temperature (°C)	Repetitions
25-0*x**	400	90	25	3
50-0*x**			50	2

* *x* is a serial number that indicates the repetition number of the test.

All of the coupons were fabricated using the same technique in order to minimize the interspecimen variability. The bonding surfaces of the two 19 mm thick x 38 mm wide steel plates were sandblasted and brushed with acetone to remove dust and soluble chemical contaminants from the surface. Two steel plates were aligned with one another end-to-end. A 1 to 2 mm gap was left between the ends of the steel plates to minimize stress transfer through end-to-end bonding of the steel plates.

The pultruded HM CFRP plates were fabricated with a pre-installed glass fiber peel-ply layer on the surface to prevent contamination of the surface during handling. The peel ply was removed and the CFRP plates were bonded to the steel plates using the Gurit Spabond 345 adhesive, a two part epoxy adhesive with a fast hardener. To maintain a uniform bond line thickness e-glass spacer beads with diameters in the range of 0.8 to 1.2 mm, produced by MoSci Corporation, were mixed into the uncured adhesive using a weight fraction of 1 gram of beads per 100 grams of adhesive. The adhesive was applied generously to the surface of the CFRP plate using a plastic spatula to minimize the formation of air voids in the adhesive layer. The CFRP plates were aligned with the steel plates and firmly pressed in place. During curing the coupons were clamped in place using mechanical clamps as shown in Figure 3.2 and allowed to cure at room temperature for at least 24 hours prior to removing the clamps. After curing of the first side of the joint, the coupon was flipped and the second side of the joint was prepared using the same technique.

3.1.2 Materials

The properties of the HM CFRP, epoxy adhesive and steel plates that were used in this study are presented in the following sections.

3.1.2.1 Steel Material Properties

The steel plates used in this study were hot rolled A36 steel with a minimum reported tensile strength of 250 MPa. Additional materials to produce tensile coupons for material testing were not available. As such, the elastic modulus of the steel was directly from the double-lap shear coupon tests. Two strain gauges (Vishay Model C2A-13-062LW-350) were affixed to either side of the steel plates reduced section 25 mm away from the end of the CFRP plate and 110 mm away from the grips. The strain gauges were positioned to be in the far field so that they would be unaffected by stress or strain concentrations near geometric discontinuities in the specimen. The measured strain, applied load and geometry were used to calculate the elastic modulus. The elastic modulus was obtained by fitting a best fit line to the test data between 15 kN and 90 kN. The results are given in the Table 2.

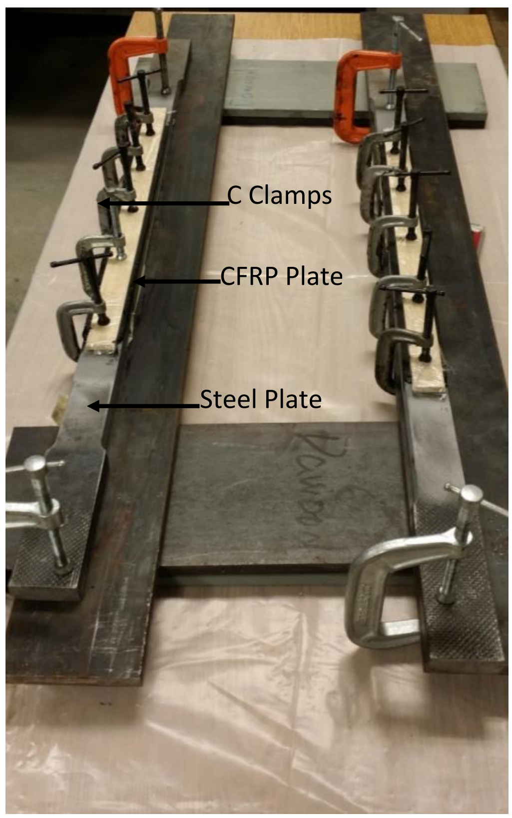

Figure 3.2 Typical double-lap shear coupon during clamping and curing

Table 2 Steel Plate Material Properties

Specimen ID	Young Modulus [GPa]
25-01	200
25-02	201
25-03	195
Average	199
SD	3.41
COV	1.72%

3.1.2.2 CFRP Material Properties

E-Plate HM1020 CFRP plates, which are distributed by Mitsubishi Plastic Composites America Inc, were used in the experimental study. The tensile properties of the CFRP plates as reported by the manufacturer are presented in Table 3.3. The as-received plates were nominally 6 m long x 100 mm wide. The plates were cut to length using a hack-saw and miter box and were cut to width using a wet-cut tile saw.

Table 3.3 HM1020 CFRP Plate Properties

	HM1020
Young`s modulus (GPa)	450
Tension strength (MPa)	1200
Thickness (mm)	2
Width	100
CFRP cross-section area (mm^2)	200
Weight (g/m)	364

3.1.2.3 Epoxy Material Properties

The epoxy adhesive used in this study was Spabond 345 with the fast hardener which is produced by Gurit. The reported glass transition temperature, T_g of the epoxy is 55^oC. This value was obtained using digital scanning calorimetry (DSC) as reported by the manufacturer. This measurement technique identifies the glass transition temperature by measuring the heat absorption of the specimen during a thermal scan. As such, the glass transition temperature measured using DSC is not based on a measurement of a mechanical property of the adhesive and may not correlate well with the mechanical response of the adhesive at elevated temperatures. Therefore, monotonic tension tests of the adhesive were conducted at different temperatures within the range of interest. Since e-glass spacer beads were used to maintain the bondline thickness of the bonded joints two batches of epoxy samples were tested, one with and one without e-glass spacer beads, to evaluate the mechanical properties of the adhesive at different test temperatures. The same fabrication and testing procedure was used for both batches of adhesive.

The material properties of the epoxy adhesive were determined at nominal temperatures of 25, 40, and 50°C. At least three epoxy tension coupons were tested according to ASTM D638-10 at each of the target test temperatures. Type II dog-bone shape tension coupons were fabricated by casting the epoxy into a non-stick plastic mold as shown in Figure 3.3. The epoxy was allowed to cure at room temperature for seven days prior to removing the coupons from the molds.

The instrumentation and test setup for the epoxy tension coupon tests are shown in Figure 3.4.The elongation of the epoxy coupon during the test was measured using a 12.7 mm gage length extensometer (Epsilon Technology Model 3442-0050-050-HT1). The applied load was measured using a 44.5 kN capacity load cell (Tovey Model# SW10-5K-B000). The epoxy coupons were tested in a custom built electromechanical loading frame. The testing temperature was controlled using a frame-mountable environmental chamber (Instron Model#3111) with a temperature range from room temperature to 204°C. Two T-type thermocouples (Omega Model SA1-T-120) were used to measure the temperature inside the chamber. One was bonded to the surface of the epoxy coupon while the other was placed inside the environmental chamber.

Figure 3.3 Epoxy coupons in plastic mold

After the environmental chamber reached the target test temperature, the epoxy coupon and the extensometer were placed inside. The bottom of the epoxy coupon was clamped in the lower grip while the top was left free to permit unrestrained thermal expansion of the adhesive. The epoxy coupon and extensometer were left in the chamber for 15 min. until the temperature of the epoxy stabilized at the target test temperature.

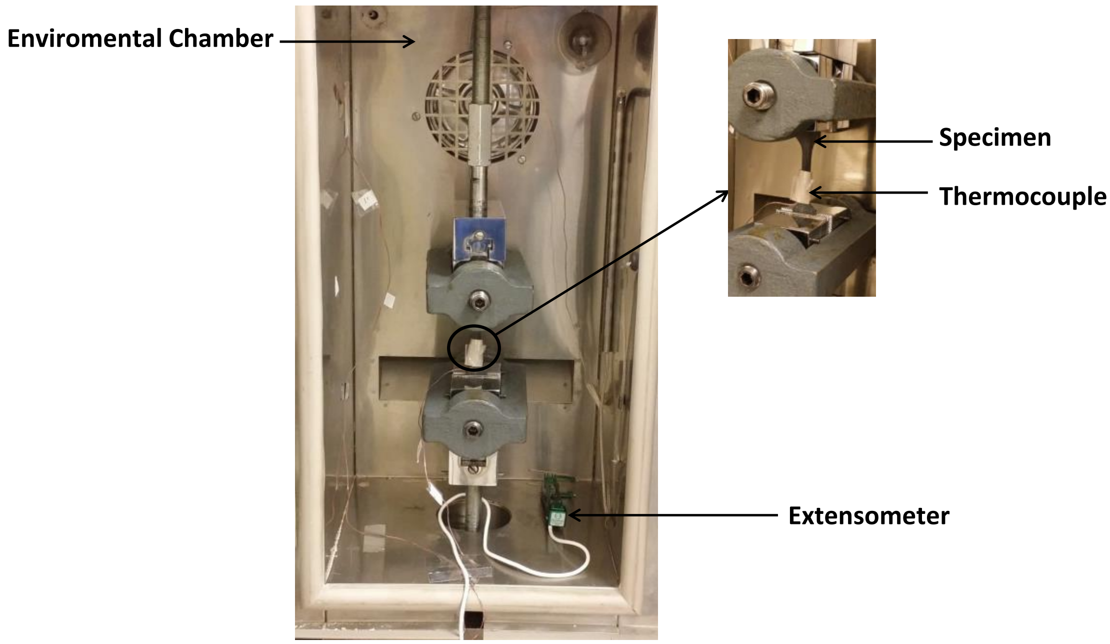

Figure 3.4 Test set up of epoxy coupon

When the measured temperature of the specimen reached the testing temperature, the environmental chamber door was briefly opened to clamp the top end of the coupon in the upper grip. The chamber was closed and the temperature was allowed to stabilize briefly. Subsequently, the epoxy coupon was monotonically tested in tension until failure.

Figure 3.5 shows the stress-strain curves of tested epoxy at different target temperatures. Inspection of the figure indicates that, at 25^{o}C the epoxy response was essentially linear and elastic and exhibited little to no plastic deformation. As the target test temperature increased, the elastic stiffness of the epoxy decreased, the inelastic strain capacity increased and the ultimate tensile strength decreased. A similar trend was observed for both sets of epoxy (with and without glass spacer beads).

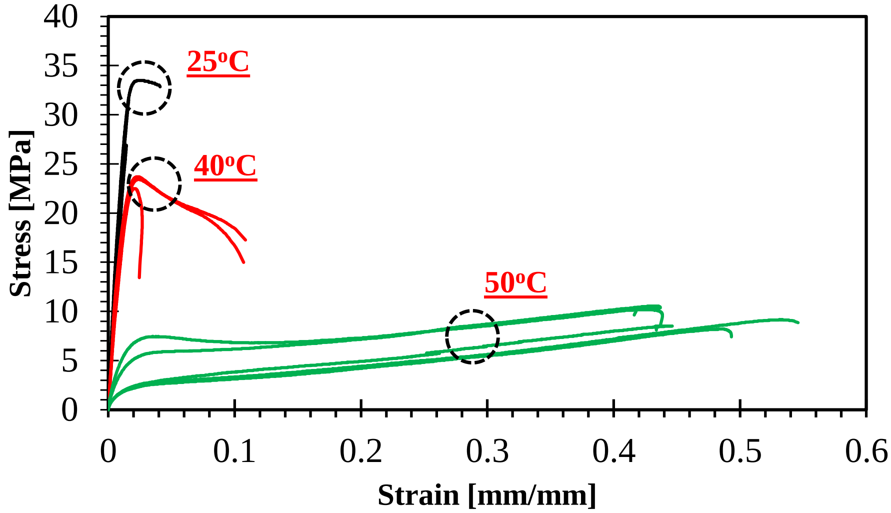

(a)

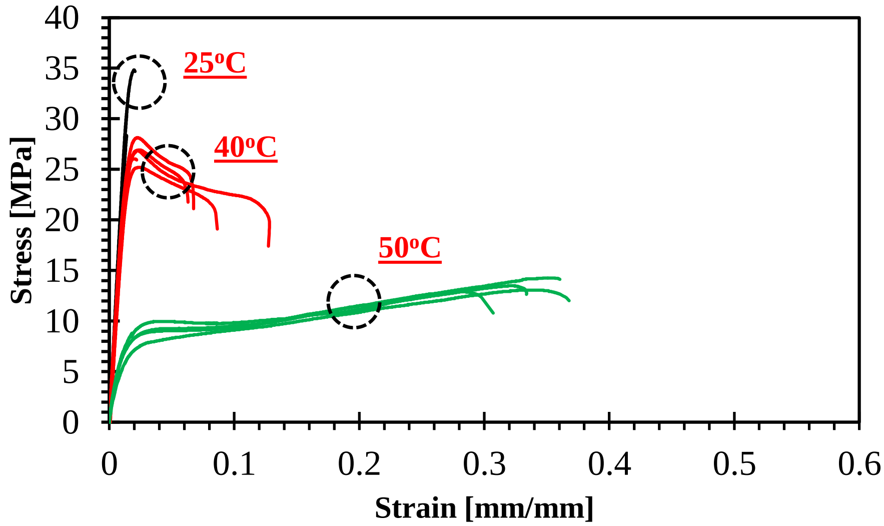

(b)

Figure 3.5 Stress Strain Curve for Spabond 345 epoxy at different ambient temperatures (a) adhesive with 1% weight content of e-glass spacer beads (b) neat adhesive without glass beads.

The measured elastic modulus, ultimate strain, ultimate tensile strength, and toughness of the epoxy at 25, 40, and 50^{o}C are shown in Table 3.4, Table 3.5, and Table 3.6.

Table 3.4 Spabond 345 Epoxy Material Properties at 25°C

Test Repetition	Measured Coupon Temperature (°C)		Elastic Modulus (MPa)		Ultimate Tensile Strain (mm/mm)		Tensile Strength (MPa)		Adhesive Toughness (MPa)	
	No Beads	With Beads	No Beads	With Beads	No Beads	With Beads	No Beads	With Beads	No Beads	With Beads
Epoxy-1	24.8	26.1	2250	2810	0.0158	0.0410	33.3	34.9	0.28	1.13
Epoxy-2	25.2	26.1	2140	2420	0.0174	0.0162	32.4	32.8	0.21	0.28
Epoxy-3	25.4	26.3	2390	2730	0.0206	0.0143	36.2	32.1	0.45	0.20
Epoxy-4	-	26.2	-	2590	-	0.0285	-	36.0	-	0.70
Average	25.1	26.2	2260	2636	0.0179	0.0250	34.0	33.9	0.31	0.58
SD	0.27	0.06	126	170	0.0024	0.01	1.98	1.80	0.12	0.43
COV	1.0%	0.2%	5.6%	6.4%	13.5%	49.6%	5.8%	5.2%	40.1%	73.8%

Table 3.5 Spabond 345 Epoxy Material Properties at 40 °C

Test Repetitions	Measured Coupon Temperature (°C)		Elastic Modulus (MPa)		Ultimate Tensile Strain (mm/mm)		Tensile Strength (MPa)		Adhesive Toughness (MPa)	
	No Beads	With Beads	No Beads	With Beads	No Beads	With Beads	No Beads	With Beads	No Beads	With Beads
Epoxy-1	41.2	40.1	1800	1970	0.0864	0.109	26.9	24.0	1.865	2.14
Epoxy-2	41.3	40.7	1730	1980	0.1282	0.027	27.4	23.4	2.844	0.40
Epoxy-3	41.6	40.5	1960	1910	0.0219	0.107	28.6	24.5	0.381	2.05
Epoxy-4	39.7	-	1880	-	0.0630	-	28.8	-	1.437	-
Epoxy-5	40.1	-	1940	-	0.0674	-	28.5	-	1.594	-
Average	40.8	40.5	1862	1955	0.0734	0.081	28.1	24.0	1.62	1.53
SD	0.80	0.34	98.87	37.2	0.04	0.047	0.85	0.566	0.88	0.98
COV	1.9%	0.8%	5.31%	1.9%	52.6%	57.8%	3.0%	2.3%	54.4%	64.0%

Table 3.6 Spabond 345 Epoxy Material Properties at 50 °C

Test Repetitions	Measured Coupon Temperature (^oC)		Elastic Modulus (MPa)		Ultimate Tensile Strain (mm/mm)		Tensile Strength (MPa)		Adhesive Toughness (MPa)	
	No Beads	With Beads	No Beads	With Beads	No Beads	With Beads	No Beads	With Beads	No Beads	With Beads
Epoxy-1	51.1	50.6	804	701	0.334	0.4386	14.3	10.1	3.560	3.38
Epoxy-2	51.4	51	762	291	0.361	0.4370	14.7	10.5	3.975	2.82
Epoxy-3	51.1	49.8	704	269	0.307	0.4462	13.4	8.5	3.276	2.30
Epoxy-4	51.2	49.6	583	311	0.368	0.4931	13.2	8.2	3.817	2.44
Epoxy-5	-	49.7	-	234	-	0.5460	-	9.2	-	2.51
Average	51.2	50.2	713	361	0.342	0.4722	13.9	9.3	3.657	2.69
SD	0.12	0.6	96.28	192.3	0.03	0.05	0.71	1.01	0.31	0.43
COV	0.2%	1.2%	13.5%	53.3%	8.1%	10.0%	5.1%	10.8%	8.3%	15.9%

The variation of the adhesive modulus, strength and toughness with temperature are plotted in Figure 3.6 (a), (b) and (c), respectively. Inspection of the figures indicates that the tensile modulus of the adhesive at 40^{o}C is 15% lower than the modulus at 25^{o}C while the tensile strength is 30% of the tensile strength at 25^{o}C. Additionally, the tensile modulus and strength of the adhesive drop significantly at 50^{o}C. However, the toughness of the adhesive increased significantly with temperature. The adhesive toughness at 40 and 50^{o}C are 2.6 and 4.6 times higher, respectively than adhesive toughness at 25 ^{o}C.

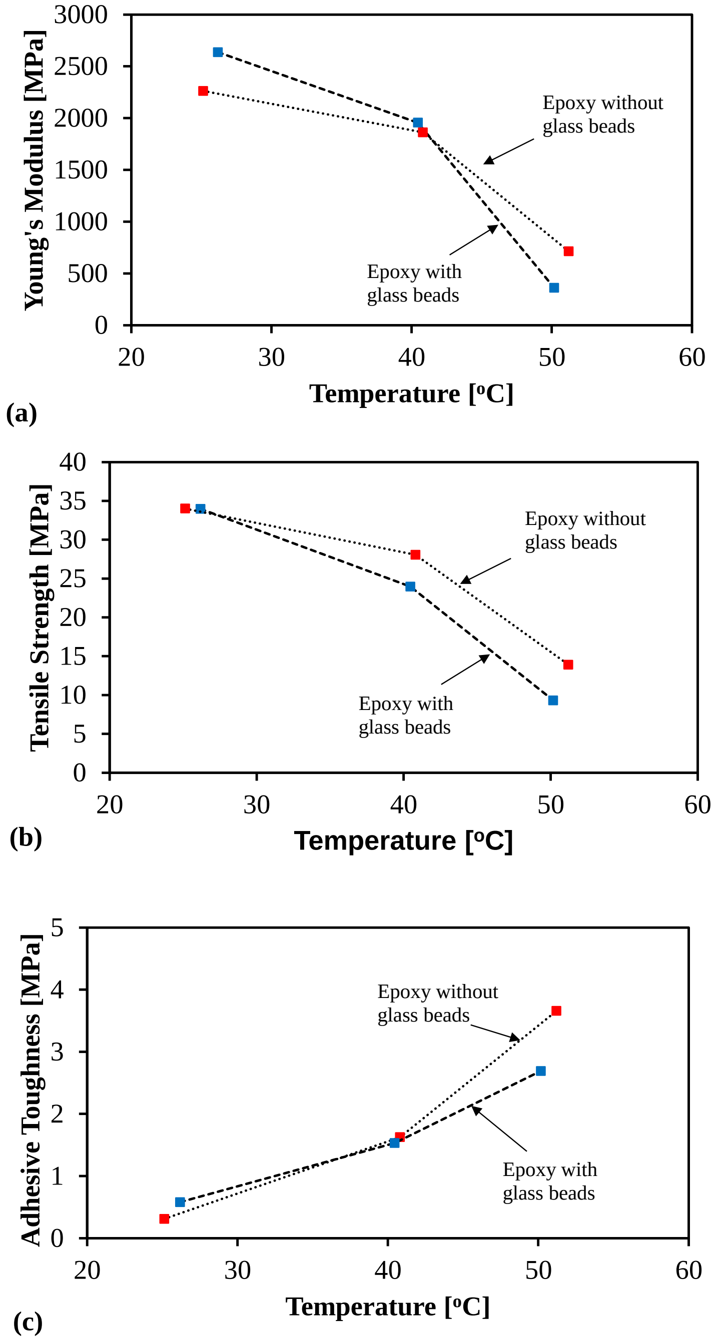

Figure 3.6 Effect of temperature on epoxy (a) Young's modulus, (b) Tensile strength and (c) Toughness

3.1.3 Test Setup and Instrumentation

All of the double-lap shear coupons were instrumented with the same number and configuration of strain gauges (Vishay Model C2A-13-062LW-350) as illustrated in Figure 3.7. Five strain gauges were placed on the CFRP plate along the longitudinal centerline of the specimen, while two strain gauges were bonded directly to the steel surface along the longitudinal centerline on either face of the specimen. Additional, strain gauges from the same batch were bonded to unstressed samples of steel and CFRP, and titanium silicate (TiS) glass for thermal correction of the gauge response. The double-lap shear coupons were also instrumented with T-type thermocouples (Omega model SAT-1-120). Data was recorded continuously using a Vishay Micromeasurements System 7000 data acquisition system with an acquisition rate of 1 Hz.

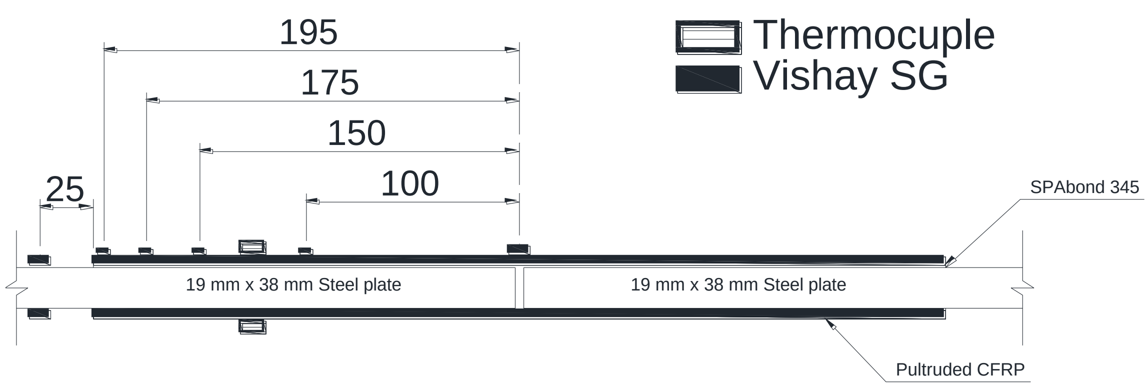

Figure 3.7 Test configuration of typical double lap shear specimen

All of the double-lap shear coupons were tested using 1200 kN Shore Western servo-hydraulic, axial-torsion universal testing machine as shown in Figure 3.8. The test temperature was maintained using an Instron environmental chamber. The coupons were placed inside the testing frame and the bottom portion of the coupon was gripped in the lower grips. The temperature of the chamber was set and the specimen was allowed to reach temperature unrestrained until the output of the strain gauges and thermocouples stabilized, approximately 75 minutes. The top of the specimen was gripped in the upper grips and the specimen was loaded until failure at a constant displacement rate of 0.1 mm/min.

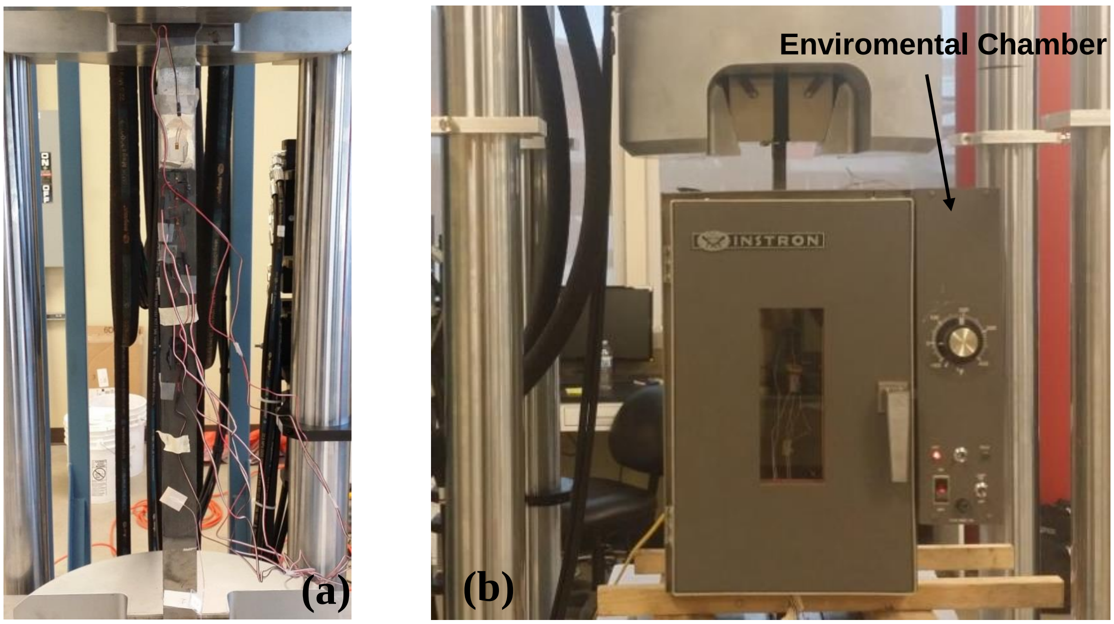

Figure 3.8 The front view of specimen (a) 25°C tests (b) 50°C tests

3.2 Steel Beam Tests

A total of 8 large-scale steel beams were strengthened with CFRP plates and tested to study their behavior under combined thermal and flexural loading conditions. The main aim of the testing was to measure the strain distributions and bond capacities of the beams and to observe the failure modes at different test temperatures. In the following sections, the details of the test specimens and test matrix, material properties, instrumentation, and test setup are presented.

3.2.1 Test Specimen and Test Matrix

A typical test beam is illustrated schematically in Figure 3.9. The tested beams consisted of a W310×38.7 (W12×26 US designation) steel beam with a C250×22.8 (C10×15.3 US designation) channel welded to the compression flange. The beams were strengthened using externally bonded HM CFRP plates that were bonded to the undersides of the tension flanges of the steel beams. All of the beams were tested in a simply supported, four point bending configuration with a span of 3048 mm and a 440 mm long constant moment region, centered on the beam midspan.

Each of the beams was strengthened with a single 100 mm wide, 4 mm thick HM CFRP plate. Three different plate lengths, 900 mm, 1800 mm, 2750 mm, were considered.

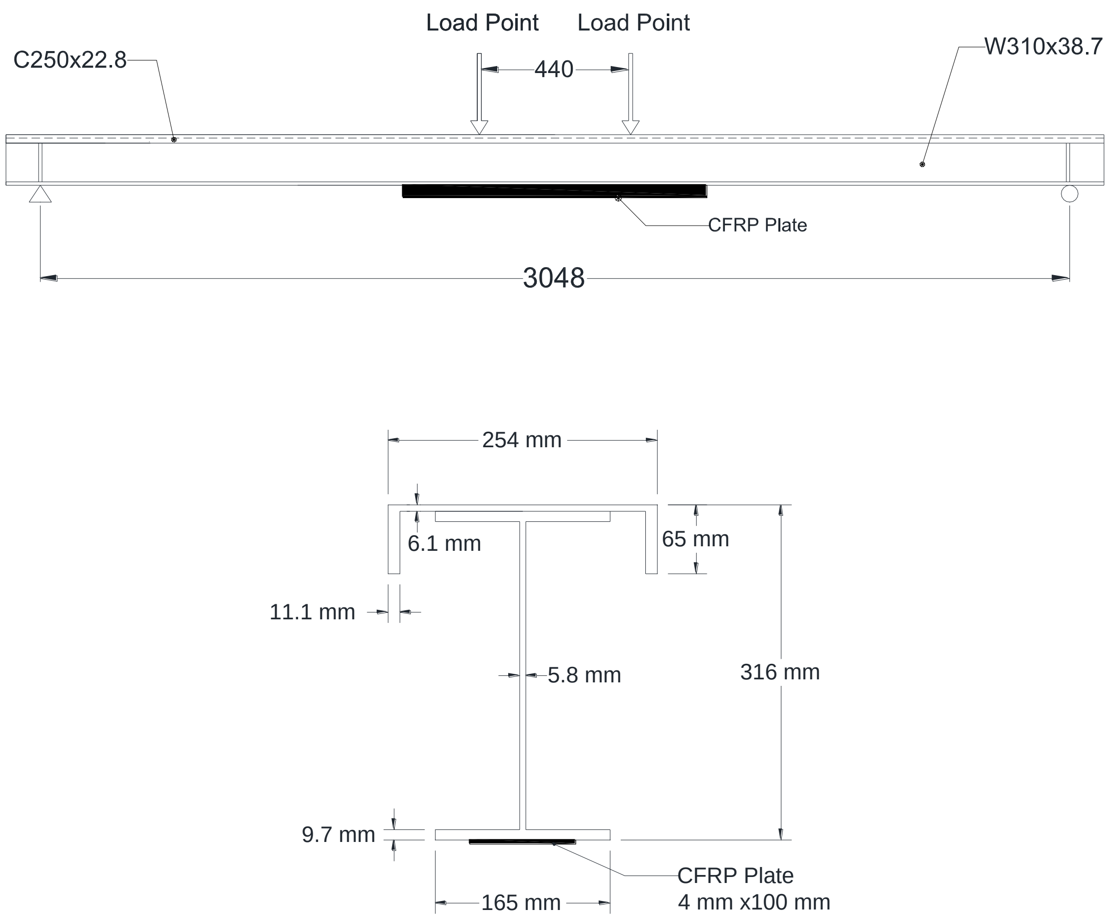

Figure 3.9 A typical steel test beam schematically

The sectional responses of the strengthened and unstrengthened beams were obtained from a moment curvature analysis as described by Dawood (2005). Based on results of the sectional analysis and considering the loading configuration and geometry of the beam, the relation between the CFRP plate length and the maximum applied load required to achieve failure of the beam was obtained as illustrated in Figure 3.10. Failure was either dominated by rupture of the CFRP in the strengthened region (for longer plate lengths) or yielding of the steel in the unstrengthened region (for shorter plate lengths).

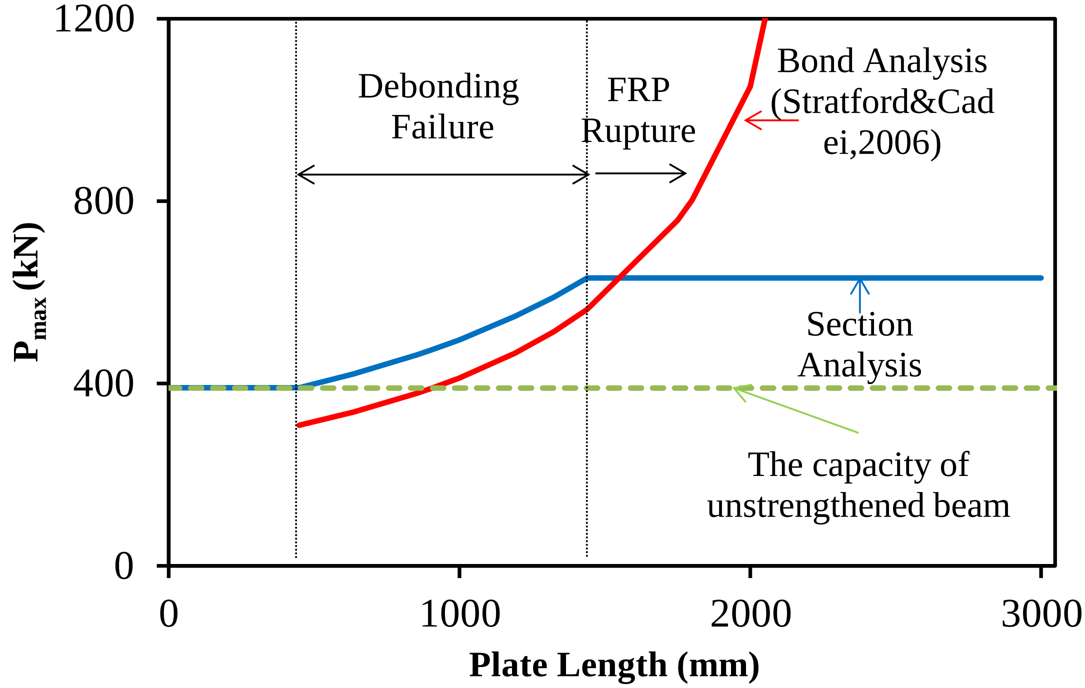

Figure 3.10 The failure load vs Plate Length Relation

The load causing debonding of the CFRP plates from the steel was predicted using the elastic bond model developed by Stratford and Cadei (2006). Based on the model, debonding occurs when the maximum principal stress in the adhesive reaches its ultimate strength. This model was used to develop a relationship between the CFRP plate length and the load causing debonding as illustrated in Figure 3.10 . The flexural capacity of the unstrengthened beam is indicated using a dashed line in Figure 3.10 for reference purposes.

Based on this analysis, three different lengths of CFRP plates were selected. The 900 mm plate length was selected so that the predict failure mode of the beam at 25^{o}C would be debonding prior to reaching the flexural capacity of the unstrengthened steel beam. The 1800 and 2750 mm plate lengths were selected so that the predicted failure mode of the beam at 25^{o}C would be rupture of the CFRP. All other failure modes, including local web crippling, local web yielding, web side-sway buckling, and lateral torsional buckling were prevented by designing appropriate stiffeners and lateral braces.

Table 3.7 summarizes the test matrix for the steel beam tests. In addition to different plate lengths, three different test temperatures, 25, 40, and 50^{o}C were considered. Test temperatures of 40 and 50^{o}C were selected to be respectively just below and just above the temperatures at which significant softening of the adhesive was observed. Each specimen was assigned a three part identifier. The first part indicates the CFRP plate length in millimeters. The second part indicates the ambient temperature in degrees Celsius. The last part indicates the repetition number of the test.

Table 3.7 The Test Matrix of Steel Beam Tests

Specimen ID	CFRP Thickness (mm)	CFRP Plate Length (mm)	Test Temperature (°C)	Repetitions
900-25-0*x**	4	900	25	2
900-40-01			40	1
900-50-01			50	1
1800-25-01		1800	25	1
1800-50-01			50	1
2750-25-01		2750	25	1
2750-50-01			50	1

*****x is the repetition number

The preparation and bonding of the CFRP plate to the steel tension flange was performed following the recommendations reported by Schnerch et al (2007).

Before installation of the CFRP plate, the bottom surface of the steel beam tension flange was sand blasted as shown in Figure 3.11 to remove rust, mill scale and debris. The sand blasted surface was cleaned using pressurized air to remove any particles remaining on the surface from the sand blasting process. After this process was completed, the steel surface was cleaned by applying acetone excessively to remove any debris or chemical residue on the steel surface.

Figure 3.11 Sandblasting of tension surface of steel beam specimen

Since the CFRP plate had a glass fiber peel ply, the peel ply was removed before spreading the epoxy on the plate surface. The CFRP plates were bonded to the steel surface within 12 hours after the sand blasting to minimize the formation of corrosion on the surface of the grit blasted steel beam. One 400 mL tube of Spabond 345 two part epoxy was emptied into a one quart plastic mixing container. E-glass spacer beads with a size of 0.8 to 1.2 mm, produced by MoSci Corporation, were added into the mixing container with a weight fraction of 1% to maintain a uniform bond line thickness. The epoxy was mixed using a plastic spatula ensuring a uniform distribution of color and glass beads in the mixed adhesive. The peel ply on the surface of the CFRP plate was removed as soon as the epoxy was completely mixed. The epoxy was applied over the surface of the CFRP plate using a 100 mm wide plastic spatula. The plate was firmly pressed on to the bottom surface of the steel tension flange and clamped in place using C clamps and a 25 mm thick x 150 mm wide padded wooden board. The clamps were left on the specimen for at least 12 hours to ensure that the epoxy set adequately before removing the clamps. Epoxy was allowed to cure at room temperature at least one week prior to testing. Figure 3.12 (a) shows the tension flange of the steel beam before bonding the CFRP plate. Figure 3.12 (b) shows a typical 900 mm long CFRP plate with the Spabond 345 before bonding to the steel beam. The clamping process of CFRP plates is shown in Figure 3.12 (c).

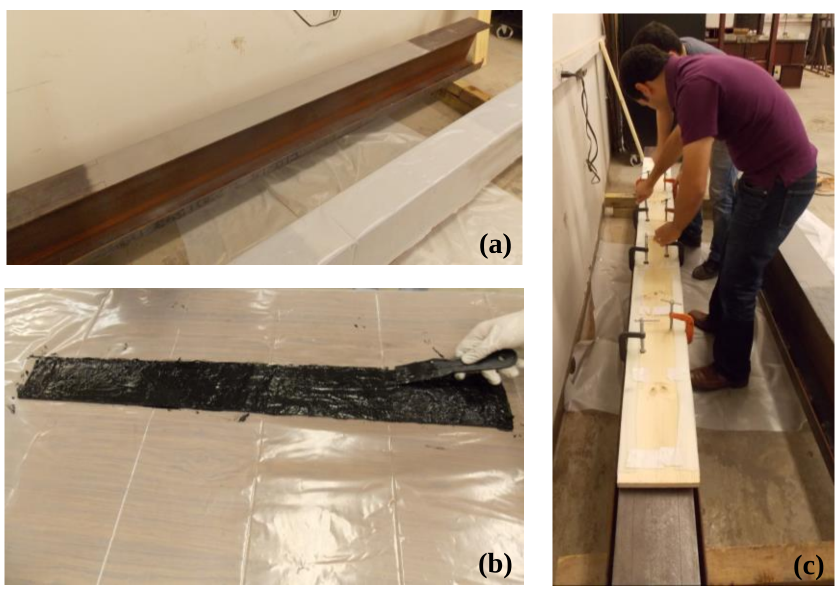

Figure 3.12 (a) The tension flange of steel beam before installation of CFRP plate (b) applying Spabond 345 epoxy to CFRP plate (c) clamping process after installation of CFRP plate

3.2.2 Materials

The adhesive and CFRP that were used for the flexural tests were the same as those used for the double-lap shear coupon tests. The adhesive properties are given in Section 3.1.2.3. The CFRP plates were similar to those used for the double-lap shear coupon tests with the exception that the plates were 4 mm thick rather than 2 mm thick. The reported properties of the CFRP are the same for both plate thicknesses.

3.2.2.1 Structural Steel

The steel beam and channel were fabricated using ASTM A992 steel. Steel coupons were fabricated by cutting from the webs of the steel beam and channels. These coupons were tested according to ASTM A370-14. Figure 3.13 presents the stress strain relationships for the steel coupons. The measured elastic modulus, yield strength and ultimate strength of the steel beam and channel are given in Table 3.8 and Table 3.9, respectively.

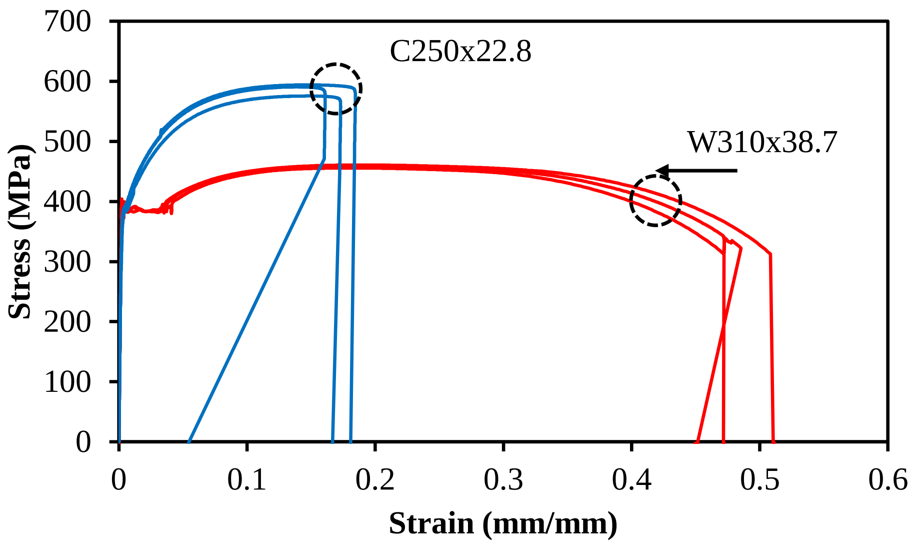

Figure 3.13 Stress-strain curves of steel beam and steel channel

Table 3.8 Steel Beam Tensile Properties

Specimen ID	Elastic Modulus (MPa)	0.2% offset Yield Strength (MPa)	Ultimate Strength (MPa)
Coupon-1	191000	383	456
Coupon-2	179000	384	461
Coupon-3	18900	386	458
Average	186000	384	458
SD	6540	1.5	2.5
COV	3.5%	0.4%	0.5%

Table 3.9 Steel Channel Tensile Properties

Specimen ID	Elastic Modulus (MPa)	0.2% offset Yield Strength (MPa)	Ultimate Strength (MPa)
Coupon-1	201000	388	594
Coupon-2	190000	381	576
Coupon-3	188000	381	591
Average	193000	383	587
SD	6870	4.0	9.6
COV	3.6%	1.1%	1.6%

3.2.3 Test Setup and Instrumentation

The beams were tested in a 900 kN-capacity self-reacting frame that was assembled inside a walk-in environmental chamber (Envirotronics Model WP813-1-7.5-WC-RUM). The frame was specially designed for the testing program and was initially assembled outside of the chamber, as shown in Figure 3.14 to validated fit-up. Load was applied using a 933-kN capacity hydraulic jack (Enerpac Model RR-10013) coupled with a 700 bar hand pump (Enerpac Model P84). Load was measured using a 900 kN load cell (Omega Model LCHD-200K).

Figure 3.14 Partially assembled 900 kN self-reacting frame before installing inside the chamber

The details of the fully assembled test set up inside the environmental chamber are shown in Figure 3.15. The beams were tested in a four point bending configuration with a span of 3048 mm and 440 mm long constant moment region. The load was applied to the beam through a steel spreader beam Steel Watts linkage lateral braces were installed to minimize lateral movement and prevent lateral torsional buckling. The lateral braces were mounted between the compression side of the steel beam and the steel reaction frame at four locations as shown in Figure 3.15.

Figure 3.15 Typical test setup for four point steel beam bending test

The environmental chamber has a temperature range of -10 to 80^{o}C and is equipped with a dedicated digital controller One T type thermocouple type (Omega SA1-T-120) was placed inside the environmental chamber to measure the ambient temperature. Two T type thermocouples (Omega SA1-T-120) were attached to the specimen. One thermocouple was bonded on the surface of CFRP plate and the second was embedded within the adhesive layer at the midspan of the beam during the fabrication process. Prior to testing, the steel beam was left inside the environmental chamber until the measured temperature inside the bond line stabilized. The specimen was then loaded to failure.

The tested beams were also instrumented with electrical resistance strain gauges and string potentiometers. The instrumentation configurations for the strengthened beams are illustrated schematically in Figure 3.16. Additional, strain gauges from the same batch were bonded to unstressed samples of CFRP and titanium silicate (TiS) glass for thermal correction of the gauge response. String potentiometers were installed to measure deflections at different points. Two string potentiometers were installed at midspan, one on either side of the beam, to measure the midspan deflection and to observe any unintentional rotation of the midspan cross-section. One string potentiometer was installed at each support to measure support settlement.

Strain gauges were bonded to the surface of the CFRP plates to measure the strains induced by thermal and mechanical loading. The strain gauges were bonded at different locations along the half length of each CFRP plate. While strain measurements were only taken on one side of the CFRP plate, previous research on bonded high modulus CFRP double-lap shear coupons and splice joints of high modulus CFRP plates bonded to steel beams indicates that the strains on the both sides of a CFRP plates are typically with 5% of one another (Dawood, 2008).

Data was collected using a Vishay Micromeasurements System 7000 data acquisition at an acquisition frequency of 1 Hz.

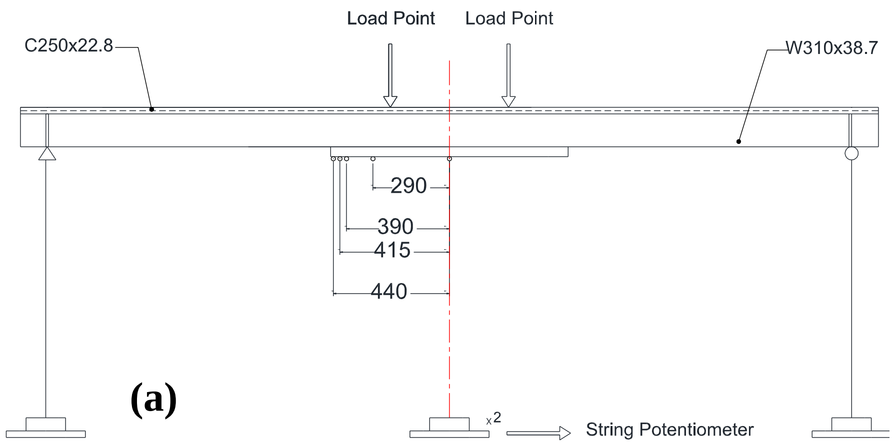

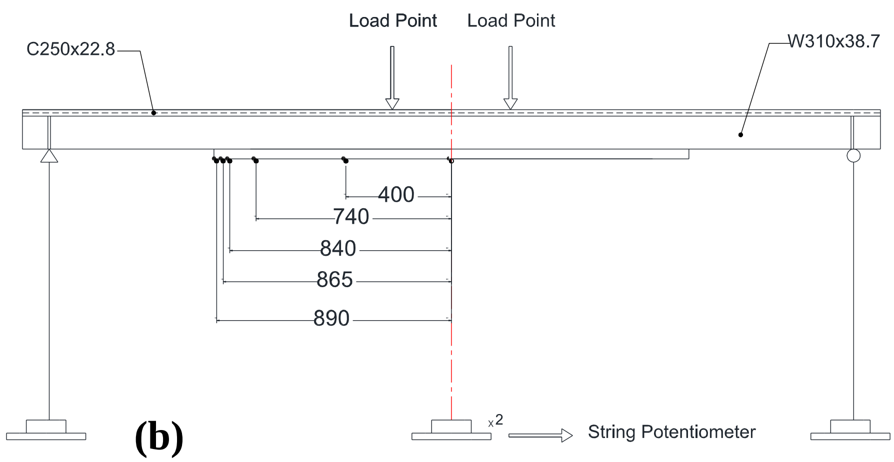

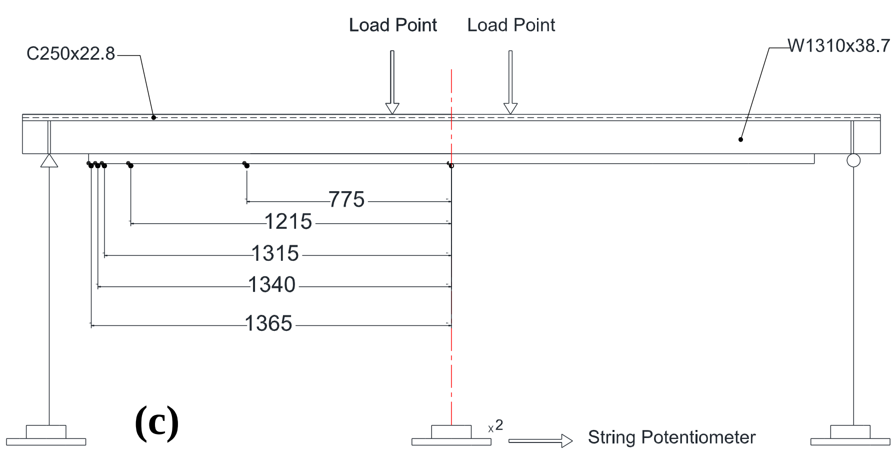

Figure 3.16 Typical string potentiometer and strain gauge locations for (a) 900 mm long CFRP plate (b) 1800 mm long CFRP plate (c) 2750 mm long CFRP plate

CHAPTER 4 EXPERIMENTAL RESULTS

This chapter presents the result of the double-lap shear coupon tests and the steel beam tests. The results and discussion of the double-lap shear coupon tests are given in section 4.1, while those of steel beam tests are presented in section 4.2

4.1 Results of the Double-Lap Shear Coupon Tests

This stage of the experimental program consisted of five double-lap shear coupon tests. Three coupons were tested at 25^{o}C while two coupons were tested at 50^{o}C. The following sections present the detailed results for each test temperature followed by a discussion. It should be noted that the data from the strain gage which is closest to the plate end for each double-lap shear coupons was eliminated because the measured strain were within the error range of the gauge. As such, the load-induced longitudinal strain in the CFRP plate at the end of the plate was taken as zero based on consideration of the free end of the plate.

4.1.1 Results of Tests at 25^{o}C

All three of the coupons that were tested at 25^{o}C failed due to sudden, brittle debonding of the CFRP plate from the steel surface as show in Figure 4.1. The failures occurred at load levels of 95.1, 96.7, and 112 kN. Inspection of the failure surface indicated that the failure occurred at the interface between the adhesive layer and the CFRP surface. The failure occurred in the resin rich layer at the surface of the FRP which is produced as a byproduct of the manufacturing process.

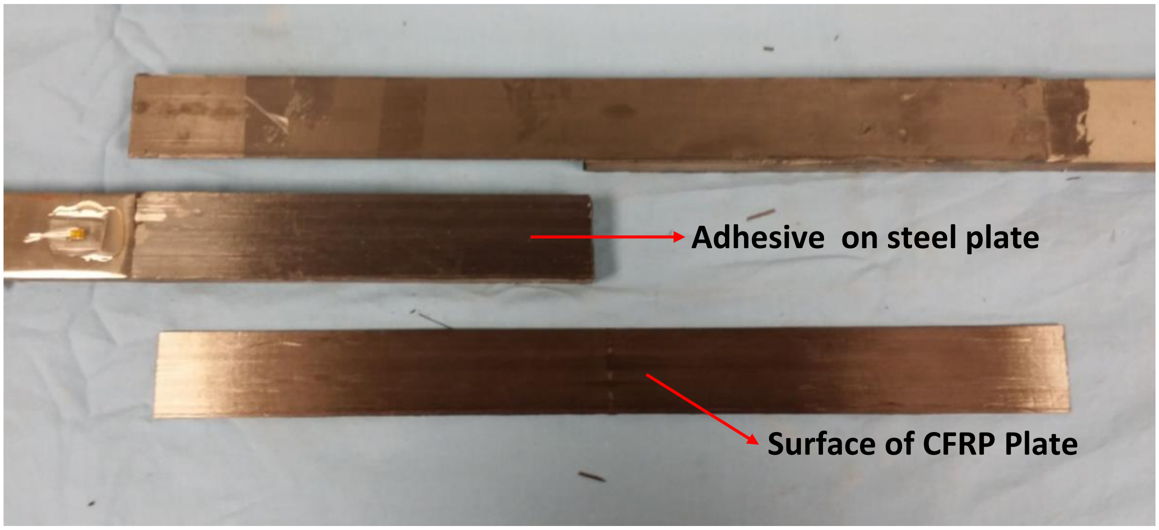

Figure 4.1 Typical failure modes for the double lap shear specimen at room temperature

The distributions of the load-induced strain in the CFRP plate were measured using electrical resistance strain gauges that were bonded to the surface of the CFRP. Strain distributions for the 25-01 coupon are plotted in Figure 4.2 at different load levels. It can be seen from the figure that the strain decreases from the center of splice to the free end at each load level. The observed trend of the strain was similar for the other coupons. The results of other two specimens are shown in the same format in Appendix A.

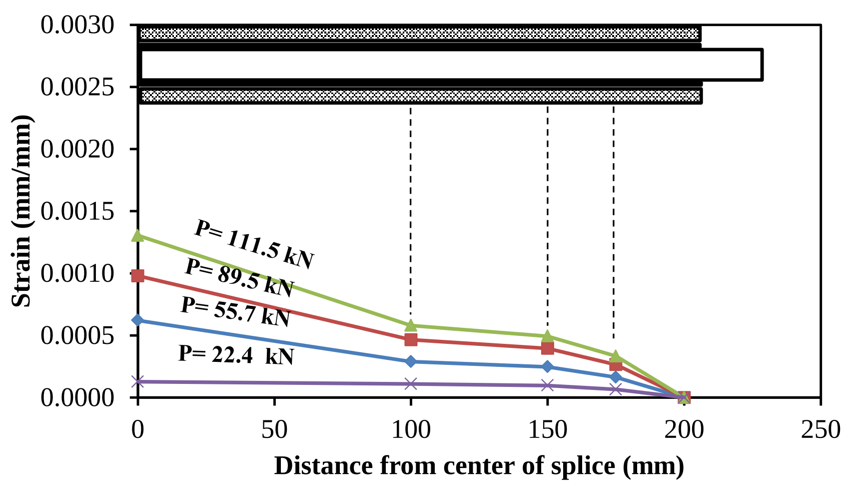

Figure 4.2 Typical longitudinal CFRP strain distributions along the bonded length

4.1.2 Results of Tests at 50^oC

Both of the coupons that were tested at 50^{o}C failed by sudden, brittle debonding of the CFRP plate from the steel surface as shown in Figure 4.3. The failure occurred at load levels of 186 and 196 kN. Inspection of the failure surface indicated that the failure occurred at the interface between the adhesive layer and the steel surface. The energy released during the sudden brittle debonding process resulted in some longitudinal splitting of the debonded CFRP.

Figure 4.3 Typical failure modes for the double lap shear specimen at 50^{o}C

The strain distributions which were induced by both mechanical and thermal loading, mechanical loading only, and thermal loading only at different load levels are shown in Figure 4.4 (a), (b) and (c) respectively. The thermally-induced strains during the heating process were calculated as

$$\varepsilon_{thermal} = \varepsilon_t - \varepsilon_{dummy} \;, \qquad (1)$$

where $\varepsilon_{thermal}$ is the thermally-induced strain, ε_t is the measured strain on the specimen during the heating process, and ε_{dummy} is the corresponding measured strain on the unstressed CFRP. The mechanically-induced-strains were calculated by subtracting the thermally-induced-strains from the measured total strains at a given load level. The maximum thermally-induced strain in the CFRP as shown in Figure 4(c) was 0.000379 mm/mm while the maximum mechanically induced strain was 0.00234 mm/mm.

The measured strains in the other coupon, which are presented in Appendix A, exhibited a similar trend.

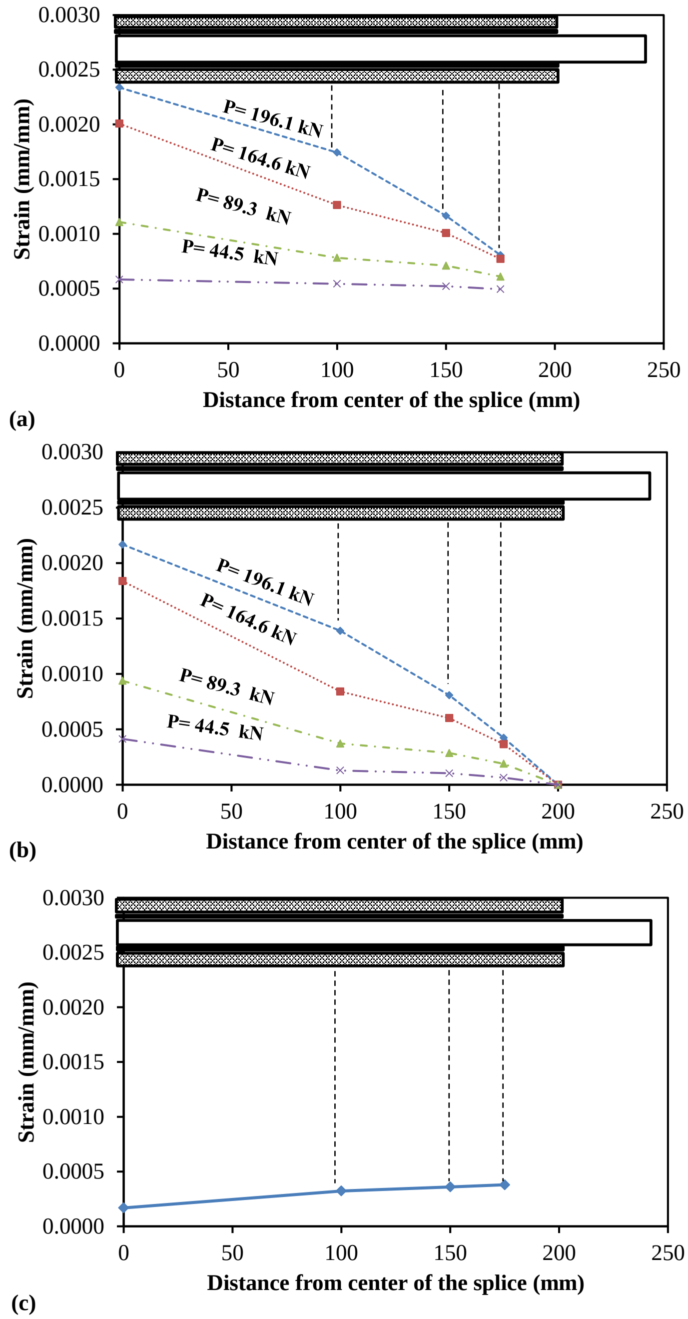

Figure 4.4 Longitudinal CFRP strain induced by (a) thermal and mechanical loading (b) mechanical loading only (c) thermal loading only

4.1.3 Discussion of Double-Lap Shear Coupons Tests

The measured load strain responses at the center of the tested double-lap shear coupons are plotted in Figure 4.5. The average debonding loads of the coupons tested at 25 and 50^{o}C were 101 and 191kN, respectively. This corresponds to a 90% increase of the average debonding load for coupons tested at 50^{o}C as compared to that of coupons tested at 25^{o}C. This is different from the trends reported in previous studies (Al-Shawaf et al., 2010; Nguyen et al., 2011). In those studies experimental results indicated that the debonding load of bonded joints decreased with increased temperatures. That trend was attributed to the lower tensile strength of the adhesive and the impact of thermally induced bond stresses in the adhesive layer due to the different coefficients of thermal expansion of the CFRP and the steel. The trend of decreasing bond strength with increasing temperature is generally supported by numerical investigations (Nguyen et al., 2011, 2012), although those investigations are generally based on elastic analyses that adopt the room-temperature mechanical properties of the adhesive to represent the mechanical properties of the adhesive at elevated temperatures.

Insight on the counterintuitive trend that was observed in this study can be obtained by considering the measured mechanical properties of the adhesive at different temperatures. The material properties reported in Section 3.1.2.3 indicate that at elevated temperatures the elastic modulus and tensile strength of the adhesive decrease compared to their room temperature values, while the inelastic strain capacity and toughness of the adhesive increase with temperature. While the reduction of strength is expected to lead to a reduction of the debonding load, this effect is counteracted by the reduced modulus, increased inelastic strain capacity, and increased toughness of the adhesive. The reduced modulus of the adhesive would lead to less severe bond stress concentrations near the end of the bonded joint while the increased inelastic strain capacity would enable redistribution of stresses away from the plate end during the loading process. In contrast, the stiff, brittle response of the adhesive at room temperature does not allow load redistribution. Finally, the increased toughness of the adhesive could possibly lead to increased energy dissipation during debonding which is, fundamentally, a fracture process.

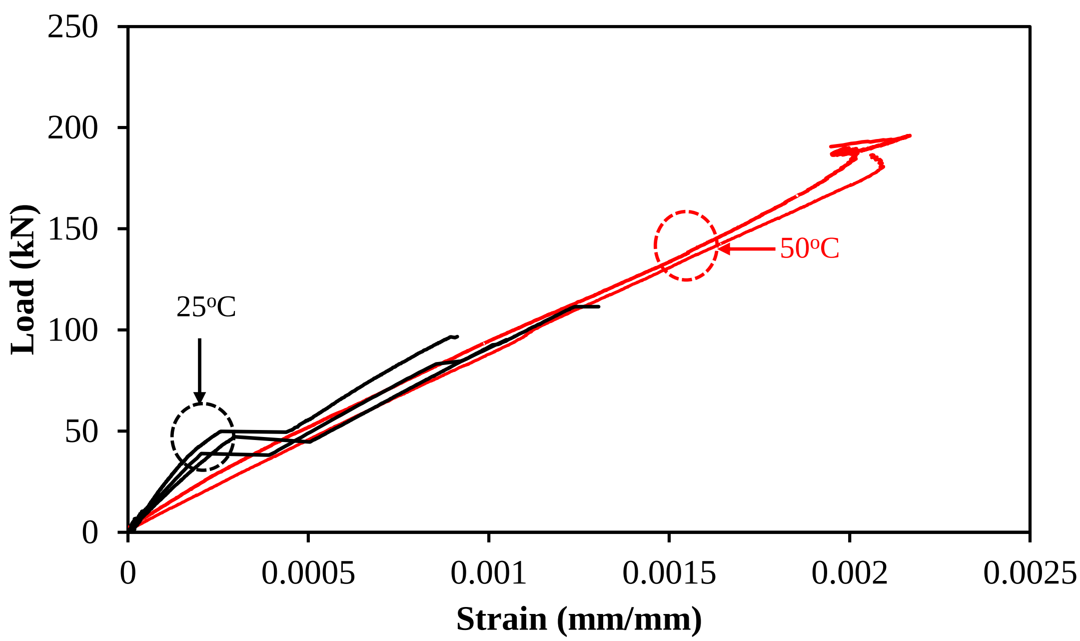

Figure 4.5. Experimental results of the ultimate tensile load- strain for double-lap shear coupons tested at 25°C and 50°C

4.2 Tests Results of the Steel Beam Test

This phase of the experimental program consisted of eight beam tests with different lengths of CFRP strengthening plates and different ambient temperatures. The results of the beam tests at 25, 40, and 50°C are presented in the following sections followed by a comparison of the results and discussion. It should be noted all data from the strain gage which is closest the plate end was eliminated since the measured strains at the location were within the error margings of the gauges. Rather, the load-induced longitudinal strains in the CFRP at the free-end of the plates were taken to be zero.

4.2.1 Results of Tests at 25^{o}C

Four beams were strengthened with different lengths of CFRP plates and tested at 25^{o}C. Figure 4.6 presents the measured load-deflection behavior of all four beams.

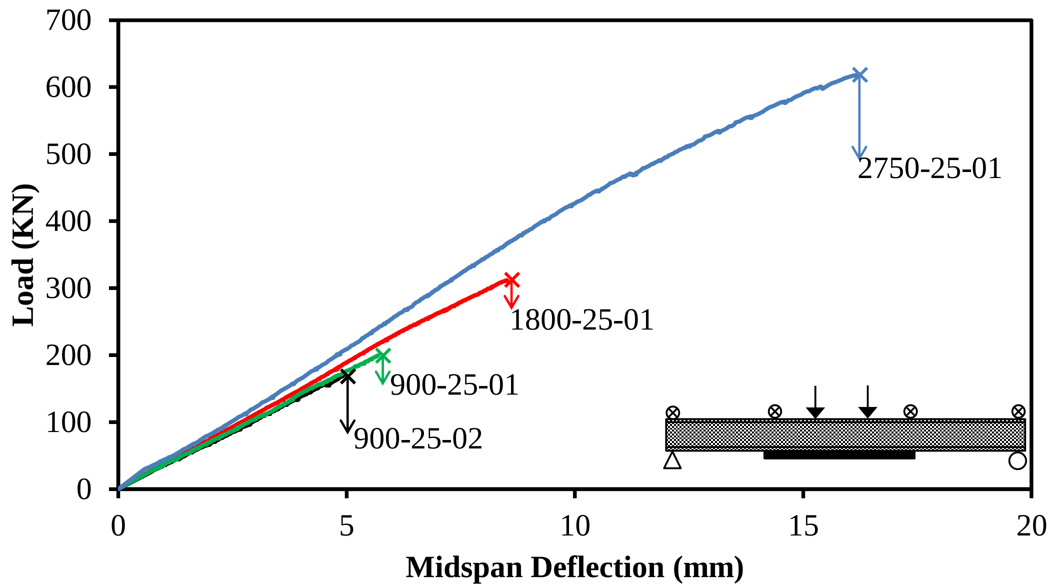

Figure 4.6 Load-deflection behavior of tested beams at 25^{o}C

It can be seen from Figure 4.6 that increasing the CFRP plate length increased the measured failure load. Beams 900-25-01, 900-25-02 and 1800-25-01 failed due to debonding of the CFRP plate, as shown in Figure 4.7, while beam 2750-25-01 failed due to rupture of the CFRP, as shown in Figure 4.8.

Figure 4.7 (a) Failure mode of 900-RT-01 (b) 900-RT-02 (c) 1800-RT-01

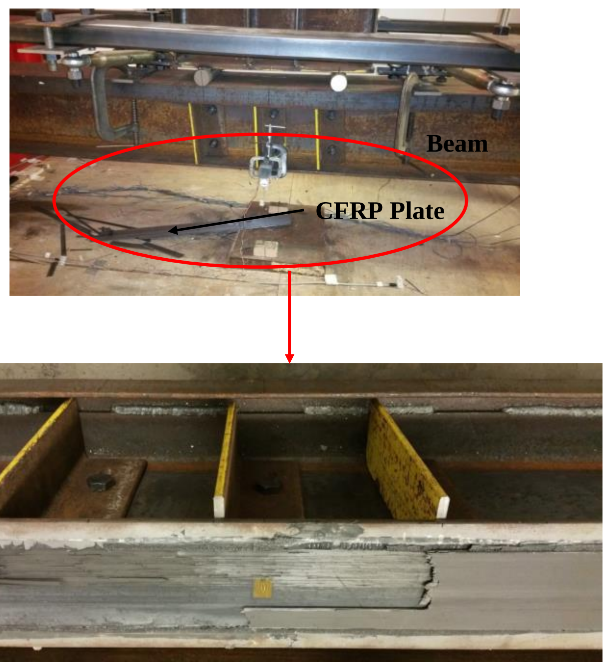

Figure 4.8 Failure modes of 2750-RT-01

Table 4.1 gives the measured failure loads of the beams and the corresponding moments at the location of the plate ends for all the tested beams. The increase in the flexural strength and shift in the failure mode was attributed to the reduction of the bending moment near the plate. The reduction of the bending moment resulted in a proportional reduction of the tension force in the steel flange which corresponds to smaller bond stresses near the plate end. Table 4.1 also lists the predicted failure load and predicted failure mode of the tested beams. Inspection of the table indicates that the elastic bond analysis does not provide an accurate prediction of the bond strength of the CFRP-steel bonded joints. While more accurate models are available, such as higher order bond analysis, or non-linear finite element analysis, these are not generally well suited for design applications. The results suggest that further research to develop accurate simplified design models to predict the bond strength is needed.

Table 4.1 The Failure Load of the Beams Tested at 25°C

Specimen ID	Predicted Failure Load (kN)	Predicted Failure Mode	Measured Failure Load (kN)	Moment at Plate End (kN-m)	Observed Failure Mode
900-25-01	388	Debonding	200	107	Debonding
900-25-02	388	Debonding	171	92	Debonding
1800-25-01	632	CFRP rupture	311	97	Debonding
2750-25-01	632	CFRP rupture	618	46	CFRP rupture

Figure 4.9 presents the measured longitudinal strain distributions at different load levels for the four strengthened beams that were tested at 25°C.

Based on the measured strain in the CFRP plate, the average shear stress in the adhesive layer between adjacent strain gauges was calculated as

$$\tau = \frac{\varepsilon_{i+1} - \varepsilon_i}{x_{i+1} - x_i} E_{CFRP} t_{CFRP} \,, \qquad (2)$$

where ε_{i+1} is the measured strain at location x_{i+1}, ε_i is the measured strain at location x_i, E_{CFRP} is the tensile modulus of the CFRP plate and t_{CFRP} is thickness of the CFRP plate. The calculated shear stress distributions in the adhesive layer due to the mechanical loading are plotted in Figure 4.9. Inspection of the figure indicates that shear stress concentration increase significantly near the plate ends.

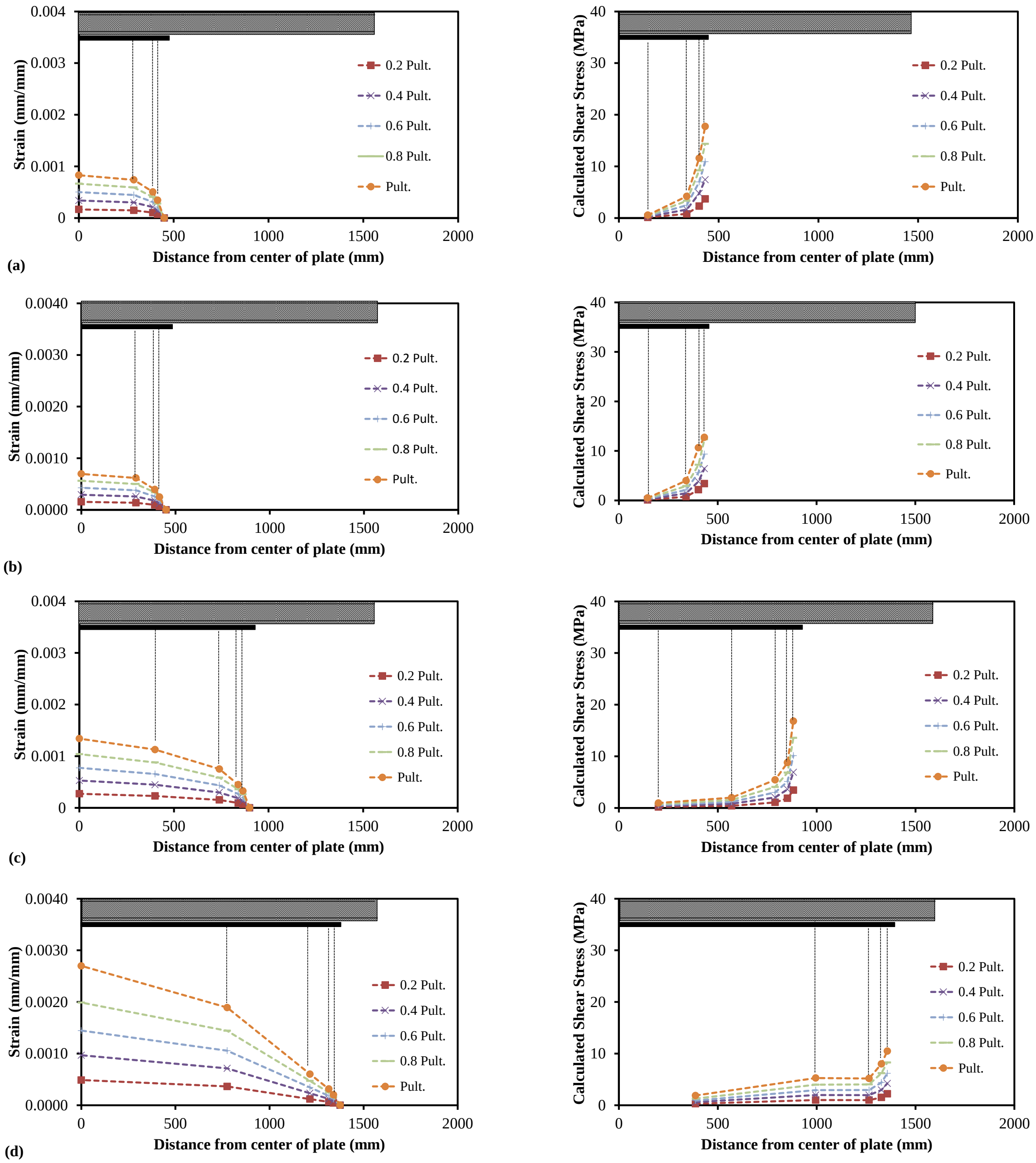

Figure 4.9 Longitudinal CFPR strain and calculated adhesive shear stress distributions along the CFRP plate for the specimen (a) 900-25-01 (b) 900-25-02 (c) 1800-25-01 and (d) 2750-25-01

Table 4.2 gives the maximum experimental adhesive shear stress at the failure load level for all the tested beams. Table 4.2 also lists the maximum predicted adhesive shear stress, peeling stress and predicted maximum principal stress proposed using the model by Stratford and Cadei (2006) at the same load level. Inspection of the table indicates that the experimental shear stresses are lower than the predicted shear stresses. It also indicates that the predicted peak principal stresses in the adhesive for beams 900-25-01, 900-25-02, and 1800-25-01, which all failed by debonding, were within 17% of one another. However, the average of the peak principal stresses was 67% of the measured room-temperature tensile strength of the adhesive. This is consistent with the observation that failure occurred in an adhesive mode at the steel-adhesive interface rather than in a cohesive mode due to material failure of the adhesive. In contrast, the maximum predicted principal stress in the adhesive for beam 2750-25-01, which failed by rupture of the CFRP plate, was half of the average of the peak principal stresses for the other three beams. In other words, the demand on the epoxy for beam 2750-25-01 was much lower than for the other specimens despite the higher failure load.

Table 4.2 The Comparison of Experimental Stresses and Predicted Stresses of the Beams Tested at 25 ^{o}C

Specimen ID	Maximum Experimental Adhesive Shear Stress (MPa)	Maximum Predicted Adhesive Shear Stress (MPa)	Maximum Predicted Adhesive Peeling Stress (MPa)	Maximum Predicted Adhesive Principal Stress (MPa)
900-25-01	17.7	32.1	14.6	25.0
900-25-02	12.8	27.4	12.5	21.3
1800-25-01	16.8	29.6	13.2	22.8
2750-25-01	10.5	16.5	6.3	12.0

The calculated shear stress distributions in the adhesive layers at the failure load levels are plotted in Figure 4.10 (a), (b), (c), and (d) for beams 900-25-01, 900-25-02, 1800-25-01, and 2750-25-01 respectively. The shear stress distributions were also predicted using the elastic bond analysis provided by Stratford and Cadei (2006). Inspection of the figure indicates that the experimental shear stresses exhibited a similar trend predicted by elastic bond analysis model.

However, the elastic bond analysis model was not used to predict the adhesive stresses for the beams tested at higher temperature because the model does not take into account the inelastic behavior of the adhesive that was observed at elevated temperature.

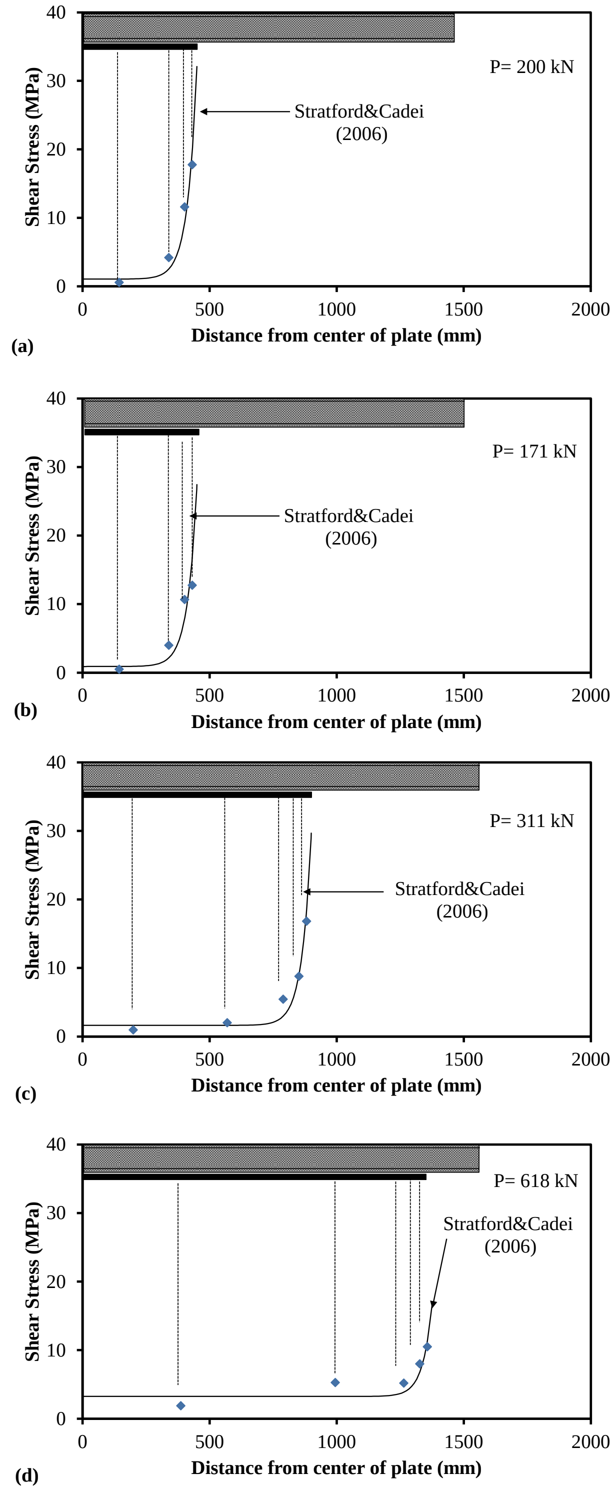

Figure 4.10 The maximum experimental and predicted adhesive shear stress distributions for the beams (a) 900-25-01 (b) 900-25-02 (c) 1800-25-01 (d) 2750-50-01

4.2.2 Results of Test at 40°C

One of the tested beams, 900-40-01, was strengthened with a 900 mm long CFRP plate and tested at 40°C. Figure 4.11 plots the measured load-deflection response. The measured failure load was 514 kN. The beam failed due to debonding of the CFRP plate. The beam remained elastic up to a load level of 401 kN. This correlates well with the predicted yielding load of the beam from the moment curvature analysis which was 401 kN. This suggests that the non-linearity of the load-deflection behavior was due to yielding of the steel rather than due to inelasticity of the epoxy.

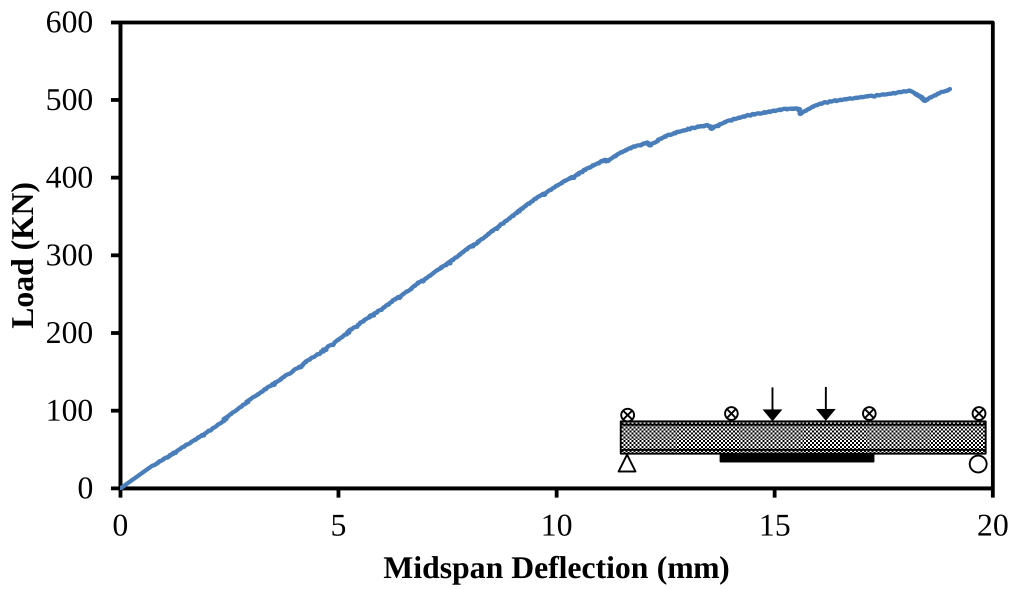

Figure 4.11 Load-deflection behavior of the specimen 900-40-01

The distribution of longitudinal strain in the CFRP plate due to combined mechanical and thermal loading is shown in Figure 4.12 (a) for different values of the applied load. The longitudinal strains due to thermal effects only were calculated as described in section 4.1.2. The distribution of longitudinal strain due to thermal effects only is plotted in Figure 4.12 (c). The maximum strain induced in the CFRP due to differential thermal expansion of the steel and the CFRP was 0.0002 mm/mm which is 7.4% of the reported rupture strain of the CFRP. The strains due to thermal loading were subtracted from the total strain to obtain the distribution of longitudinal strain due to mechanical loading only which is plotted in Figure 4.12 (b).

The average shear stress in the adhesive layer was calculated as described in the previous section. The calculated shear stress distributions in the adhesive layer due to combined thermal and mechanical loading, due to mechanical loading only and due to thermal loading only are plotted in Figure 4.12 (a), (b) and (c), respectively. Inspection of the figure indicates that the maximum calculated shear stress due to thermal loading only was 5.3 MPa which is 15% of the maximum calculated shear stress due to the combined thermal and mechanical loading. This suggests that the effect of thermally-induced bond stresses may not be as severe as previous numerical studies have suggested (Schnerch, 2005; Stratford and Cadei, 2006).

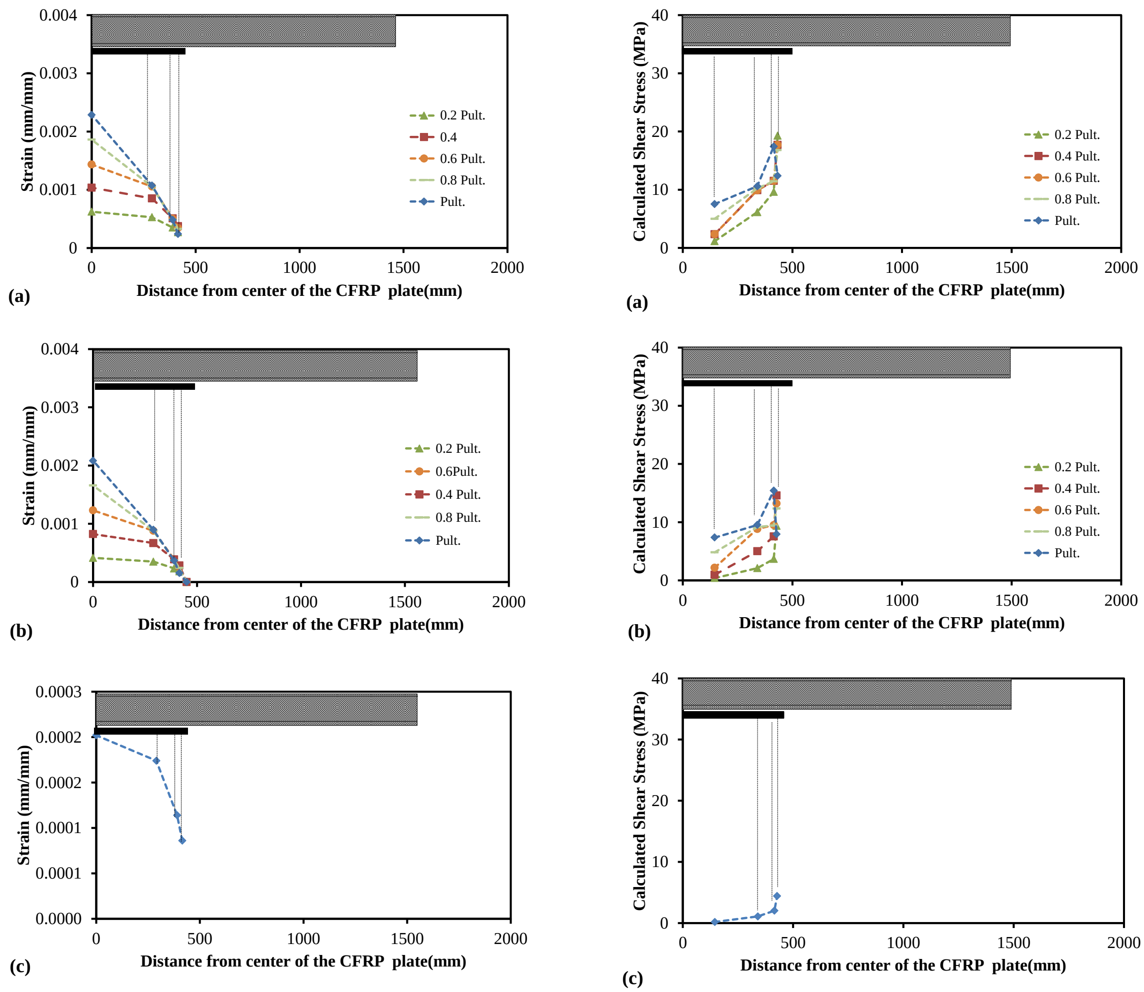

Figure 4.12 Strain and calculated shear distributions induced by (a) mechanical and thermal loading (b) mechanical loading only (c) thermal loading only

4.2.3 Results of Tests at 50^{o}C

Three beams were strengthened with different lengths of CFRP plates and tested at 50^{o}C. Figure 4.13 presents the measured load-deflection behavior of all three specimens.

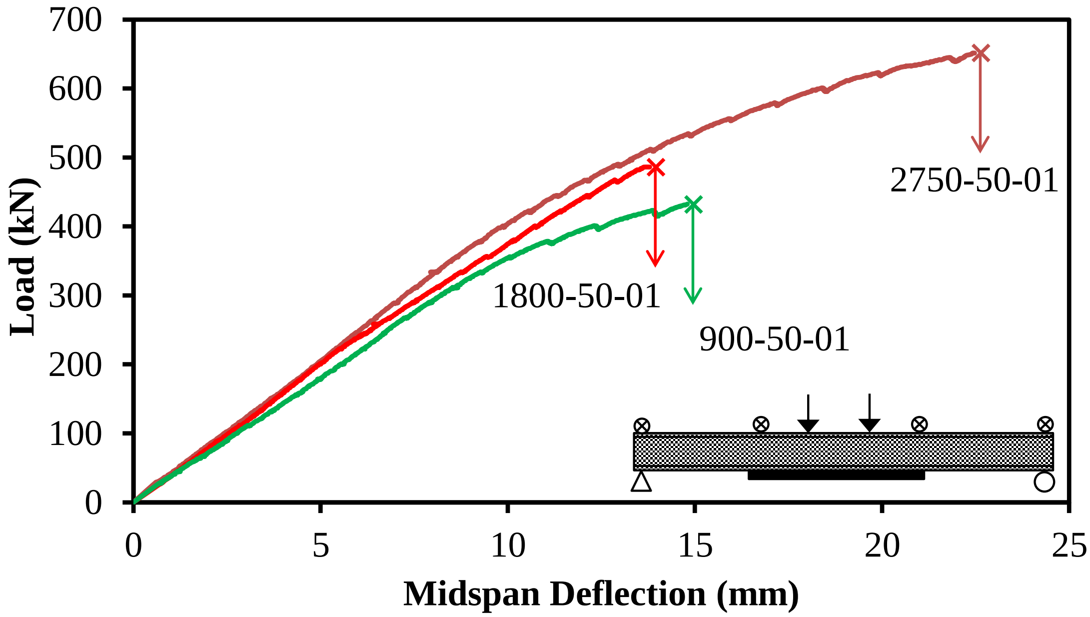

Figure 4.13 Load-deflection behaviors of tested beams 50^{o}C

The measured failure load of beams 900-50-01, 1800-50-01 and 2750-01 were 432, 486, and 651 kN, respectively. The two tested beams which were strengthened with 900 and 1800 mm long CFRP plates failed due to debonding of the plate from the steel beam. However, the beam that was strengthened with a 2750 mm long CFRP plate failed due to rupture of the CFRP. Figure 4.14 shows the failure of the three beams.

Figure 4.14 (a) Debonding failure of the specimen 900-50-01 (b) debonding failure of the specimen 1800-50-01 (c) rupture failure of the specimen 2750-50-01

The total strain due to combined mechanical and thermal loading is plotted in Figure 4.15(a) for beam 900-50-01. The strain distribution in the CFRP plate due to mechanical loading at different load levels is also shown in Figure 4.15(b). The strain distributions induced by only thermal loading are plotted Figure 4.15 (c). The maximum thermally-induced strain was 0.000039 mm/mm, which is 2.5% of the total strain due to combined thermal and mechanical loading. The results for beams 1800-50-01 and 2750-50-01 are given in the same format in Appendix A.

The total calculated shear stress due to combined mechanical and thermal loading is plotted in Figure 4.15 (a) for beam 900-50-01. The maximum shear stress induced due thermal loading was 0.18 MPa, which is 1.5% of the maximum shear stress due to mechanical loading as shown in Figure 4.15 (b). The distribution of the calculated shear stress due to thermal loading only is shown in Figure 4.15 (c). The results for the other two beams tested at 50°C are presented in similar format in Appendix A.

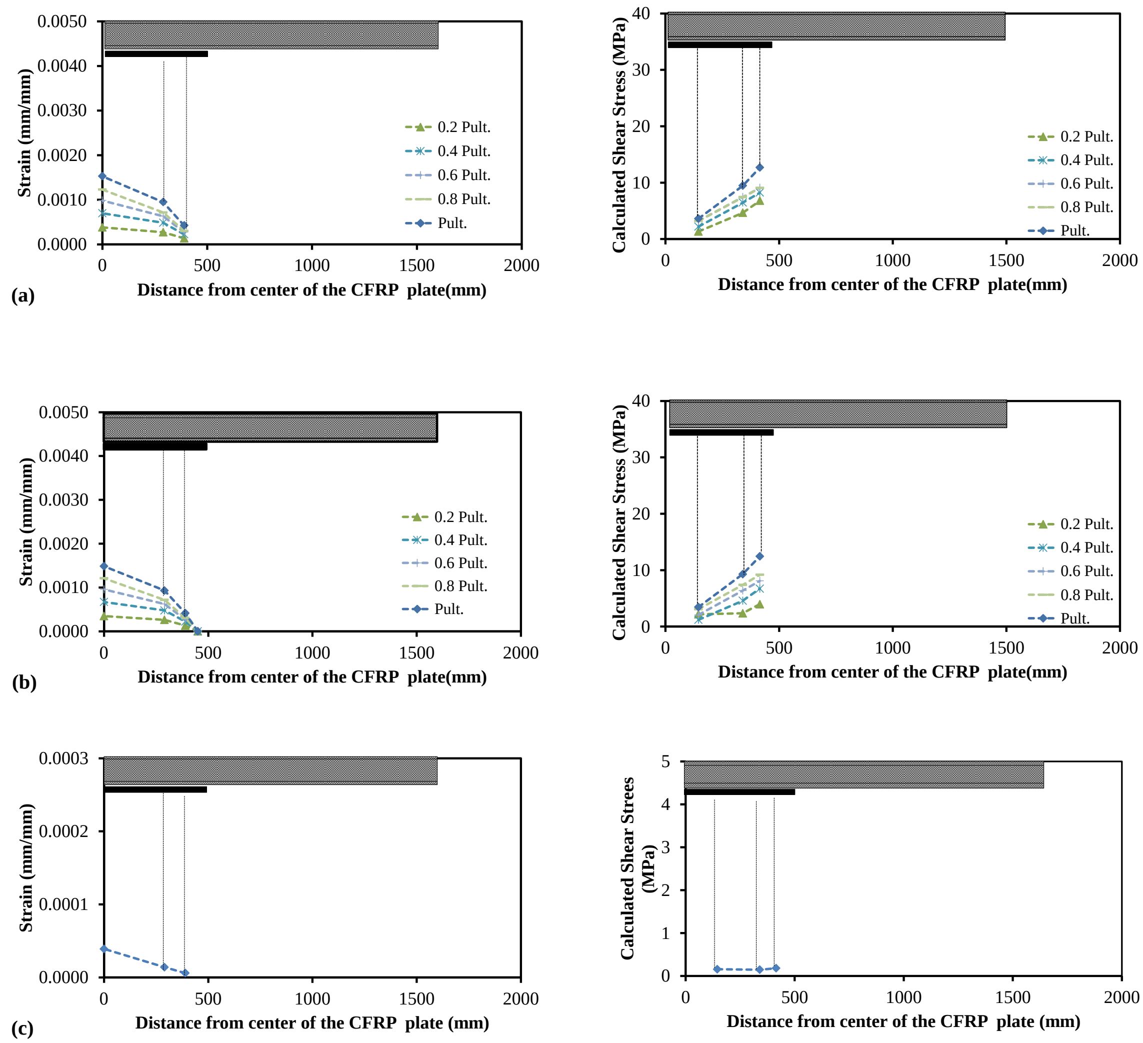

Figure 4.15 Longitudinal CFRP strain and calculated adhesive shear distributions due to (a) mechanical and thermal loading (b) mechanical loading only (c) thermal loading only for beam 900-50-01

4.2.4 Comparison of Steel Specimens Tested at Different Temperature

This part of the experimental study included three different CFRP plate lengths tested at three different temperatures. Table 4.3 summarizes the measured failure loads of the tested beams the corresponding maximum moments (in the constant moment region) and the moment at the plate end. Table 4.3 also presents the ratio of the maximum moment, M_{max} to the calculated plastic capacity of the unstregthened beam, $M_{p,un.}$

Table 4.3 Test Results of the Steel Beam Tests with Different CFRP Plate Length at Different Temperature

Specimen ID	Failure Load (kN)	M_{max} (kN-m)	Moment at Plate End (kN-m)	$M_{maximum}$ / $M_{p,un}$
900-25-01	200	130	107	0.49
900-25-02	171	112	92	0.43
1800-25-01	311	203	97	0.77
2750-25-01	618	403	46	1.52
900-40-01	514	335	276	1.26
900-50-01	432	282	232	1.07
1800-50-01	486	317	152	1.19
2750-50-01	651	424	48	1.60

Comparison of the calculated maximum moments for the beams tested at room temperature on Table 4.3 indicates that increasing the CFRP plate length increased the flexural capacity of the beams.

Figure 4.16 plots the relationship between the plate length and the measured failure load of the strengthened beam for different test temperatures. Inspection of the figure indicates a consistent trend that beams tested at 50°C exhibited higher failure loads than beams tested at 25°C. This is notable since the reported glass transition temperature of the adhesive was 55°C while the adhesive softened significantly between 40 and 50°C. Material level tests indicated that the average strength and stiffness of the adhesive at

50^oC were 73 and 85% lower than the values at 25^oC. Previous studies suggest that thermally-induced shear stresses in the adhesive layer of strengthened beams may be of comparable magnitude to the load-induced shear stresses under service conditions (Deng et al. 2004; Schnerch, 2005; Stratford and Cadei 2006). However, the test results presented in the previous sections indicate that the thermally-induced shear stresses are much lower than the load induced stresses. This is attributed to two main factors. First, the reduced elastic modulus of the adhesive at 50^oC results in a substantially lower shear stress concentration near the plate end. It is also notable that the average toughness of the adhesive at 50^oC is 4.6 times greater than the toughness of the adhesive at 25^oC. This increased toughness could increase the fracture energy required to propagate an unstable debonding crack, although this should be examined in more detail in the light of the adhesive rather than cohesive nature of the debonding failures that were observed. These factors collectively are believed to contribute to the increase of the observed debonding capacity of the tested beams at 50^oC.

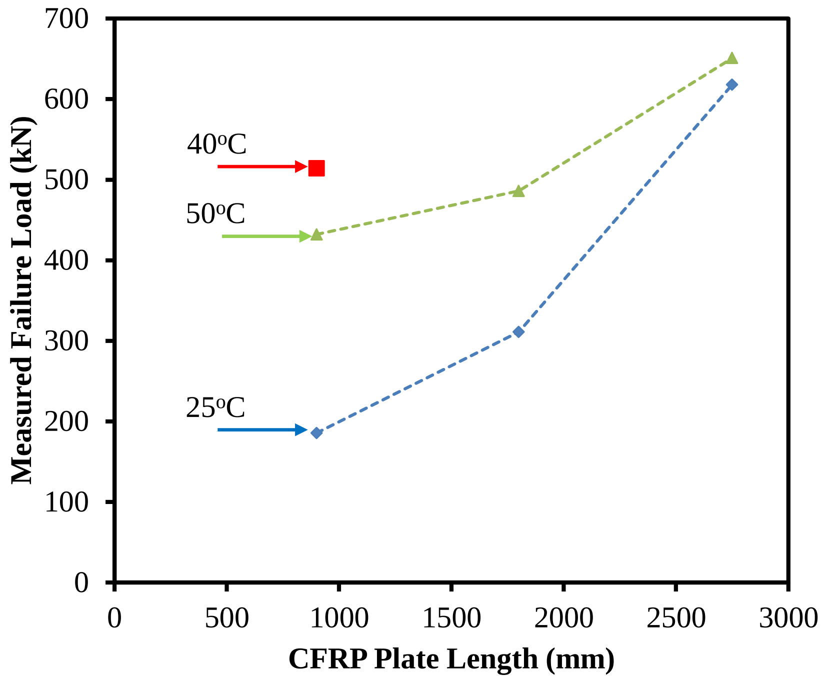

Figure 4.16 Measured failure load with different length of CFRP at different ambient temperatures

Beams 2750-25-01 and 2750-50-01 both failed by rupture of the CFRP. The capacity of beam 2750-50-01 was 5% higher than that of its room temperature counterpart. The relatively small difference of the failure load is likely due to slight differences in the material properties of the CFRP, steel, or adhesive or variations of loading and beam geometry.

Beam 900-40-01 was tested at 40^{o}C, slightly below the softening temperature of the adhesive. The failure load of beam 900-40-01 was 19% larger than the failure load of beam 900-50-01 which was tested just above the softening temperature of the adhesive. The results of this test are not consistent with the observed trend of increasing debonding load with increasing temperature. At 40^{o}C the adhesive exhibits considerable toughness, has a lower modulus than at 25^{o}C, and still retains 70% of its 25^{o}C strength. It is possible that the combination of relatively high strength and toughness and relatively low stiffness leads to the observed increase in debonding strength as compared to the beam tested at 50°C. However, additional research is needed to further investigate this behavior.

Figure 4.17 (a) – (c) present the load-deflection behavior of the tested beams strengthened with plates that are 900, 1800, and 2750 mm long, respectively. Comparison of the load-deflection behavior of the beams with similar plate lengths but tested at different temperatures indicates that increasing the ambient temperature did not have a significant effect on the stiffness of the tested beams, regardless of the plate length. This suggests that the adhesive layer retains sufficient stiffness at elevated temperatures to provide complete composite interaction between the steel and the CFRP to validate the "plane sections remain plane" assumption. For the beams strengthened with 900 and 2750 mm long plates, the inelastic stiffnesses did begin to diverge, but this occurred at load levels that are well above the expected service load levels.

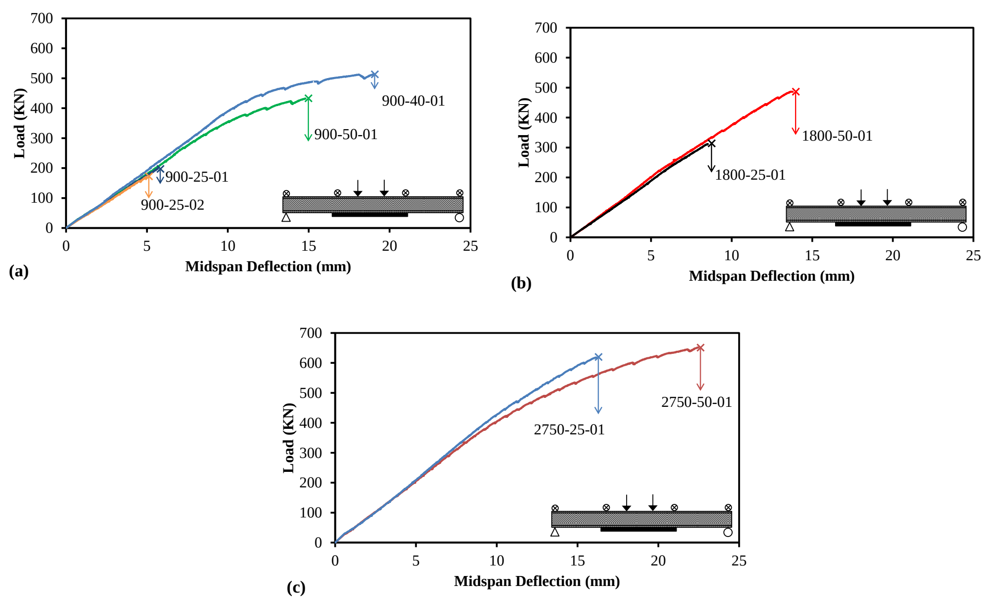

Figure 4.17 Total applied load vs midspan deflection at different temperatures for (a) 900 mm long CFRP plate (b) 1800 mm long CFRP plate (c) 2750 mm long CFRP plate

CHAPTER 5 CONCLUSIONS AND FUTURE WORK

This thesis presents the findings of an experimental program that was conducted to investigate the behavior of steel beams strengthened with high modulus CFRP plates and tested at moderately elevated temperatures, up to 50^{o}C. The experimental program was conducted in two stages. In the first stage five double-lap shear coupons were tested at 25 and 50^{o}C to investigate the effect of temperature on the debonding strength of CFRP-steel bonded joints. In the second stage, eight steel beams were strengthened with externally bonded CFRP plates of different length ranging from 900 to 2750 mm and tested at temperatures of 25, 40, and 50^{o}C to study the effect of temperature on the flexural behavior of strengthened beams. The research findings lead to the following conclusions:

- Increasing the ambient test temperature from 25 to 50^{o}C increased the toughness, and decreased the strength and stiffness of the tested adhesive by 364, 73, and 85% respectively.
- The dominant failure mechanism for all of the tested double-lap shear coupons was debonding. Debonding occurred at the CFRP-adhesive or steel-adhesive interfaces and increasing the test temperature shifted the failure location from adhesive-CFRP interface to the adhesive-steel interface.
- Test results indicate that increasing the test temperature from 25 to 50^{o}C increased the debonding load of the tested double-lap shear coupons by 89%. This increase was attributed to three factors:
    i. The decreased stiffness of the adhesive decreased the intensity of the bond stress concentrations near the plate end.

ii. The increased inelastic capacity of the adhesive allowed for redistribution of stresses away from the plate end prior to debonding.

iii. The increased toughness of the adhesive resulted in an increase of the energy required for debonding crack initiation and growth, although this should be evaluated in detail in light of the adhesive rather than cohesive nature of the observed debonding failures.

- The results of the steel beam tests indicated that the failure modes of the strengthened beams depended on the length of the strengthening plate. Beams strengthened with longer plates failed by rupture of the CFRP while beams strengthened with shorter plates failed by debonding of the CFRP from the steel surface. Beams strengthened with shorter plates experienced higher bending moments near the plate ends at a given load level which resulted in larger bond stress concentrations leading to debonding.
- The predicted adhesive shear stress distributions that were obtained using the elastic bond analysis proposed by Stratford and Cadei (2006) closely matched the experimentally-obtained adhesive shear stresses for beams tested at room temperature. The average of the predicted maximum principal stresses in the adhesive layers at the failure loads for the beams that failed by debonding was 67% of the measured adhesive tensile strength. This is consistent with the adhesive rather than the cohesive nature of the observed debonding failures. This findings suggests that further consideration needs to be given to the influence of

the adhesive-steel and adhesive-CFRP interfaces on the debonding capacity of the bonded joints.

- The debonding capacities of the beams that were strengthened with 900 and 1800 mm long CFRP plates were 116 and 56% greater than the debonding capacities of their 25^{o}C counterparts. This increase was attributed to the increase of the toughness, decrease of the stiffness, and increase of the inelastic strain capacity of the adhesive with increased temperature.

The following recommendations for future research are proposed:

- Other researchers have demonstrated that using tapered plate and reversed-tapered plate end geometries significantly reduce the stress concentration that form near the plate end. The effect of temperature on the debonding strength of plates with different plate end geometries should be investigated in detail.
- This research focused on a single type of epoxy adhesive and single type of FRP plate. Different types of epoxy and FRP should be studied to help draw more general conclusions.
- Only one beam was tested in this research at 40^{o}C. That beam had a plate length of 900 mm. Among the beams tested with 900 mm long strengthening plates, the beam tested at 40^{o}C exhibited the highest capacity, nearly 20% greater than the capacity of a similar beam tested at 50^{o}C. Further investigation is needed to clarify the reason for this observation.
- A detailed thermomechanical finite element analysis should be conducted to simulate the behavior of the beams and to develop a numerical platform through which a parametric study can be conducted.

- This research focused on testing beams at moderately elevated temperatures up to 50^{o}C. The effect of low temperatures, thermal cycling, and thermally-induced creep should be investigated in detail.

REFRENCES

Al-Shawaf, Ahmed, Al-Mahaidi, Riadh, and Zhao, Xiao-Ling. (2010). "Effect of Elevated Temperature on Bond Behaviour of High Modulus CFRP/Steel Double-Strap Joints," *Australian Journal of Structural Engineering*, 10(1), 63-74.

ASTM International. (2014). "A 370-14 Standard Test Methods and Definitions for Mechanical Testing of Steel Products," West Conshohockend, PA.

ASTM International. (2010). " D 638-10 Standard Test Method for Tensile Properties of Plastics," West Conshohockend, PA.

Dawood, M.M.R. (2005). "Fundamental Behavior of Steel Concrete Composite Beams Strengthened with High Modulus Carbon Fiber Reinforced Polymer (CFRP) Materials," (Master's Thesis, North Caroline State University, 2005).

Dawood, M., Rizkalla, S., & Sumner, E. (2007). "Fatigue and Overloading Behavior of Steel-Concrete Composite Flexural Members Strengthened with High Modulus CFRP Materials," *Journal of Composites for Construction*, 11(6), 659-669.

Dawood, M.M.R. (2008). "Bond Characteristics and Environmental Durability of CFRP Materials for Strengthening Steel Bridges and Structures," (Doctoral Dissertation, North Caroline State University, 2008).

Deng, J., Lee, M., and Moy, S. (2004). "Stress Analysis of Steel Beams Reinforced with a Bonded CFRP Plate," *Composite Structures*, 65(2), 205-215.

Deng, J., and Lee, M. (2007). "Behaviour Under Static Loading of Metallic Beams Reinforced with a Bonded CFRP Plate," *Composite Structures*, 78(2), 232-242.

Fawzia, S., Al-Mahaidi, R., & Zhao, X. (2006). “Experimental and Finite Element Analysis of a Double Strap Joint Between Steel Plates and Normal Modulus CFRP,” *Composite Structures*, 75(1-4), 156-162.

Fawzia, S., Zhao, X., & Al-Mahaidi, R. (2010). “Bond-Slip Models for Double Strap Joints Strengthened by CFRP,” *Composite Structures*, 92(9), 2137-2145.

Hollaway, L., and Cadei, J. (2002). “Progress in the Technique of Upgrading Metallic Structures with Advanced Polymer Composites,” *Progress in Structural Engineering and Materials*, 4(2), 131-148.

Harries, K., & Dawood, M. (2012). “Behavior and Performance of Fiber-Reinforced Polymer-to-Steel Bond,” *Transportation Research Record: Journal of the Transportation Research Board*, 2313(1), 181-188.

Narmashiri, K., Ramli Sulong, N., and Jumaat, M. (2011). “Flexural Strengthening of Steel I-Beams by Using CFRP Strips,” *International Journal of Physical Sciences*, 6(7), 1620-1627.

Narmashiri, K., Ramli Sulong, N., and Jumaat M. (2012). “Failure Analysis and Structural Behavior of CFRP Strengthened Steel I-Beams,” *Construction and Building Materials*, 30, 1-9.

Nguyen, T., Bai, Y., Zhao, X., and Al-Mahaidi, R. (2011). “Mechanical Characterization of Steel/CFRP Double Strap Joints at Elevated Temperatures,” *Composite Structures*, 93(6), 1604-1612.

Nguyen, T., Bai, Y., Al-Mahaidi, R. and Zhao, X. (2012). "Time-Dependent Behavior of Steel/CFRP Double Strap Joints Subjected to Combined Thermal and Mechanical loading," *Composite Structures,* 94(5), 1834-1845.

Rizkalla, S., Dawood, M., and Schnerch, D. (2008). "Development of a Carbon Fiber Reinforced Polymer System for Strengthening Steel Structures," *Composites Part A-Applied Science and Manufacturing,* 39(2), 388-397.

Schnerch, D.A. (2005). "Strengthening of Steel Structures with High Modulus Carbon Reinforced Polymer (CFRP) Materials," (Doctoral Dissertation, North Caroline State University, 2005).

Schnerch, D., Dawood, M., Rizkalla, S., Sumner, E., and Stanford, K. (2006). "Bond Behavior of CFRP Strengthened Steel Structures," *Advances in Structural Engineering,* 9(6), 805-817.

Schnerch, D., Dawood, M., Rizkalla, S., and Sumner, E. (2007). "Proposed Design Guidelines for Strengthening of Steel Bridges with FRP Materials," *Construction and Building Materials,* 21(5), 1001-1010.

Stratford, T., and Cadei, J. (2006). "Elastic Analysis of Adhesion Stresses for the Design of a Strengthening Plate Bonded to a Beam," *Construction and Building Materials,* 20(1-2), 34-45.

Stratford, T., and Bisby, L. (2012). "Effect of Warm Temperatures on Externally Bonded FRP Strengthening," *Journal of Composites for Construction,* 16(3), 235-244.

Wu, C., Zhao, X., Duan, W., & Al-Mahaidi, R. (2012). “Bond Characteristics Between Ultra High Modulus CFRP Laminates and Steel,” *Thin-Walled Structures*, 51, 147-157.

Xia, S.H. and Teng, J.G. (2005). “Behaviour of FRP-to-Steel Bonded Joints,” *Proceedings of the International Symposium on Bond Behaviour of FRP in Structures (BFFS 2005)*

Yu, T., Fernando, D., Teng, J., & Zhao, X. (2012). “Experimental Study on CFRP-to-Steel Bonded Interfaces,” *Composites Part B-Engineering*, 43(5), 2279-2289.

Zhao, X., and Zhang, L. (2007). “State-of-the-art review on FRP Strengthened Steel Structures,” *Engineering Structures*, 29(8), 1808-1823.

Zhao, X., Bai Y., Al-Mahaidi, R., and Rizkalla, S. (2014). “Effect of Dynamic Loading and Enviromental Conditions on the Bond Between CFRP and Steel: State-of-the-Art Review,” *Journal of Composites for Construction*, 18(3), 1808-1823.

APPENDIX.A Detailed Results of the Double Lap Shear Specimen Tests

The detailed results of the double lap shear specimens tested at different temperature and details of the steel beam tests are present in this appendix.

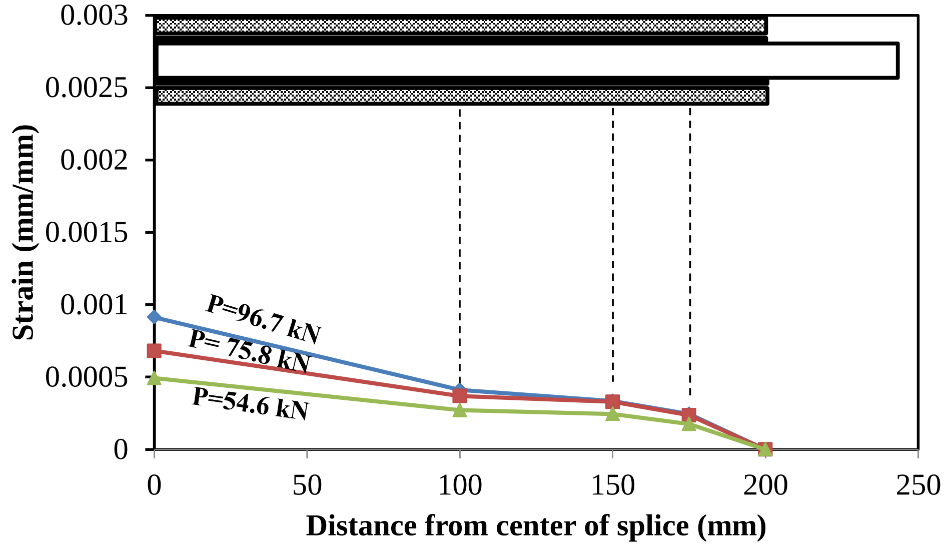

Figure A.1. Longitudinal CFRP strain distributions along the bonded length at different load level for the specimen 25-02

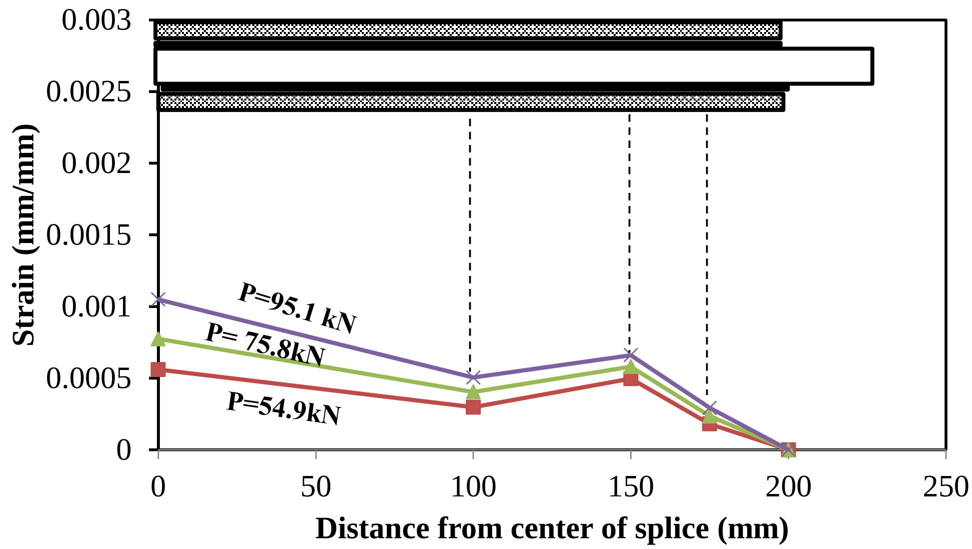

Figure A.2. Longitudinal CFRP strain distributions along the bonded length at different load level for the specimen 25-03

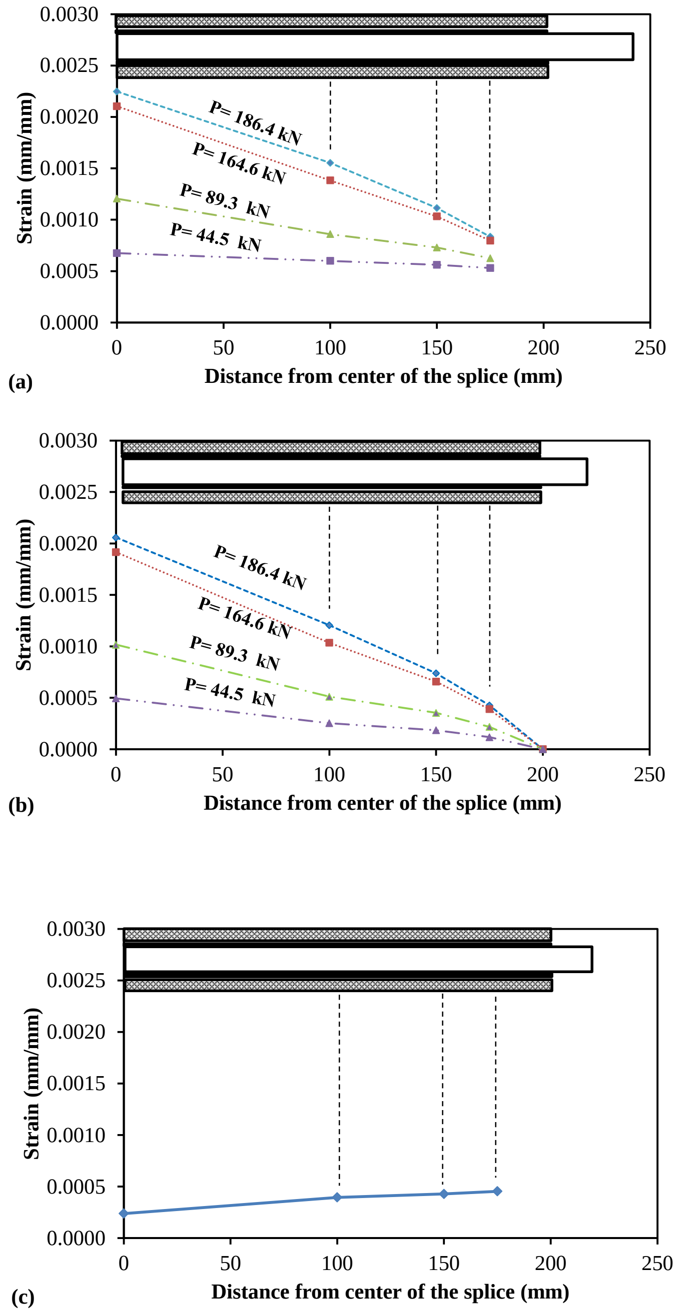

Figure A.3. Longitudinal CFRP strain induced by (a) thermal and mechanical loading (b) mechanical loading only (c) thermal loading only for specimen 50-02

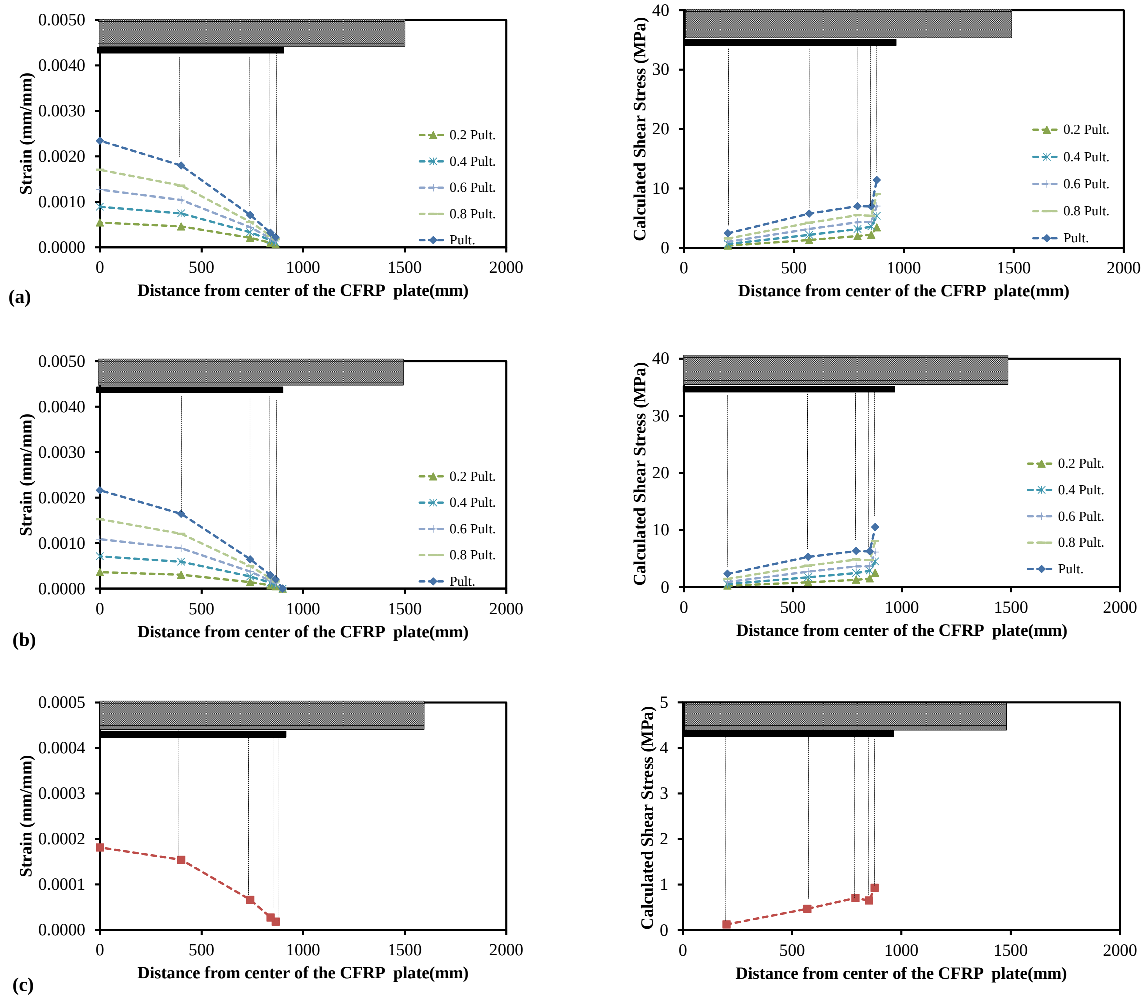

Figure A.4 Strain and calculated shear distributions induced by (a) mechanical and thermal loading (b) mechanical loading only (c) thermal loading only for beam 1800-50-01

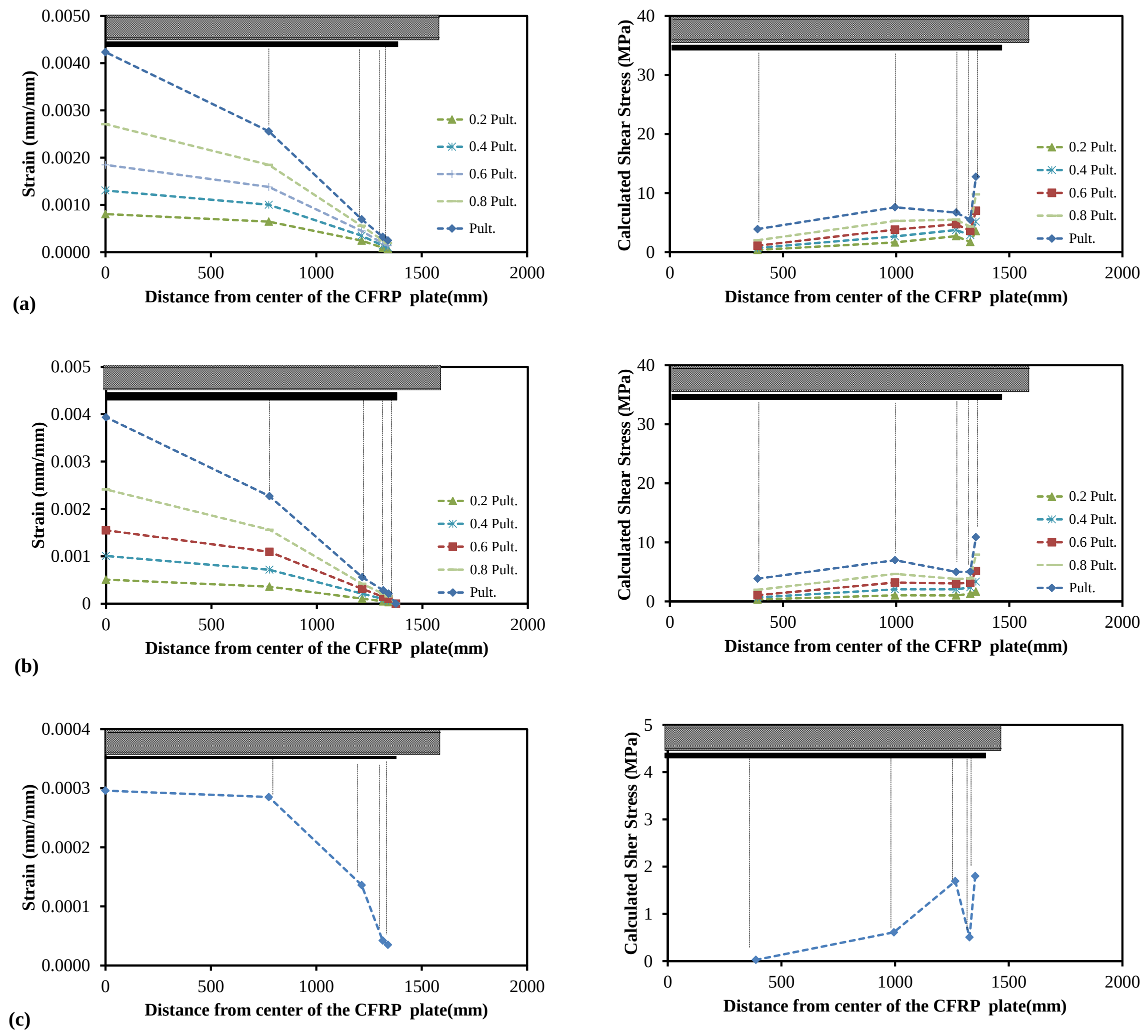

Figure A.5 Strain and calculated shear distributions induced by (a) mechanical and thermal loading (b) mechanical loading only (c) thermal loading only for beam 2750-50-01